REPORT DOCUMENTATION PAGE

Form Approved
OMB No. 0704-0188

1. AGENCY USE ONLY (Leave blank)	2. REPORT DATE	3. REPORT TYPE AND DATES COVERED
	FEBRUARY 1993	FINAL 01/15/87--11/15/92

4. TITLE AND SUBTITLE

AN EFFICIENT NUMERICAL METHOD FOR THREE DIMENSIONAL-HYPERSONIC FLOW

5. FUNDING NUMBERS

C: F33615-86-C-3015
PE: 61102
PR: 2307
TA: N6
WU: 12

6. AUTHOR(S)

ROBERT W. MACCORMACK

7. PERFORMING ORGANIZATION NAME(S) AND ADDRESS(ES)

STANFORD UNIVERSITY
DEPARTMENT OF AERONAUTICS AND ASTRONAUTICS
STANFORD CA 94305

8. PERFORMING ORGANIZATION REPORT NUMBER

9. SPONSORING/MONITORING AGENCY NAME(S) AND ADDRESS(ES)

FLIGHT DYNAMICS DIRECTORATE
WRIGHT LABORATORY
AIR FORCE MATERIEL COMMAND
WRIGHT-PATTERSON AFB OH 45433-7562

10. SPONSORING/MONITORING AGENCY REPORT NUMBER

WL-TR-93-3012

11. SUPPLEMENTARY NOTES

12a. DISTRIBUTION/AVAILABILITY STATEMENT

APPROVED FOR PUBLIC RELEASE; DISTRIBUTION IS UNLIMITED.

12b. DISTRIBUTION CODE

13. ABSTRACT *(Maximum 200 words)*

The present paper presents an efficient algorithm for solving the unsteady Navier-Stokes equations. It is a line Gauss-Seidel relaxation implicit algorithm for three-dimensional flow. Such algorithms have shown very fast convergence properties for two-dimensional flow. The extension to three-dimensions has been troublesome. The proposed algorithm presented herein was developed to solve these difficulties. A computer program based upon this algorithm has been written to solve two-dimensional plane symmetric, axisymmetric or three-dimensional flow of a perfect gas, or a real gas model for air with five species (N2, 02, NO, N, 0) or seven species (N2, 02, NO, NO^+, N, O, e^-). The program can simulate a gas in thermal equilibrium or in thermal nonequilibrium with two temperatures (Translational-Rotational and Vibrational) or three temperatures (Translational, Rotational, and Vibrational). Convergence to engineering accuracy is generally achieved in under a hundred time steps for both two- and three-dimensional flow. Provision is made within the program for a one or two equation turbulence model. Applications are presented to verify the code by comparison with experiment and flight tests. Finally, the numerically simulated flow about a hypersonic vehicle at Mach 25 in powered flight is presented.

14. SUBJECT TERMS

Computational Fluid Dynamics, Navier-Stokes Equations, Hypersonic Flow, Real Gas Effects

15. NUMBER OF PAGES

33

16. PRICE CODE

17. SECURITY CLASSIFICATION OF REPORT	18. SECURITY CLASSIFICATION OF THIS PAGE	19. SECURITY CLASSIFICATION OF ABSTRACT	20. LIMITATION OF ABSTRACT
UNCLASSIFIED	UNCLASSIFIED	UNCLASSIFIED	UNLIMITED

ACKNOWLEDGEMENTS

The author wishes to acknowledge the financial support for this work from the Department of the Air Force under contract No. F33615-86-C-3015, and Dr. J. Eric Holcomb of the Boeing Aerospace Company for his assistance in using his three dimensional grid generation procedures [see J.E. Holcomb, "Development of a Grid Generator to Support 3-D Multizone Navier-Stokes Analysis," AIAA Paper No.87-0203, 1987]. All figures were prepared using the TECPLOT plotting software of Amtec Engineering Inc.

CONTENTS

Acknowledgements	ii
List of Figures	iv
Introduction	1
Governing Equations	3
Numerical Method	4
Dissipation	8
Difficulties at Shocks	9
Stability	10
Computational Results	10
Lobb Test Case	11
RAM-C II Flight Measurements	11
Generic Hypersonic Vehicle	13
Conclusion	14
References	16
Figures	18

LIST OF FIGURES

1. Computational mesh for Lobb test case..... 18
2. Comparison of shock wave locations, Lobb test case..... 18
3. Pressure contours, Lobb test case..... 19
4. NO mass fractions, Lobb test case..... 19
5. Stagnation streamline temperature profiles, Lobb test case.. 20
6. Translational temperature contours..... 20
7. Rotational temperature contours..... 21
8. Vibrational temperature contours..... 21
9. Computational mesh, RAM-C test case..... 22
10. Pressure contours, RAM-C test case..... 22
11. Stagnation streamline temperature profiles, RAM-C test case 23
12. Stagnation streamline mass fractions, RAM-C test case..... 23
13. N_2 mass fraction contours, RAM-C test case..... 24
14. O_2 mass fraction contours, RAM-C test case..... 24
15. Translational temperature contours, RAM-C test case..... 25
16. Rotational temperature contours, RAM-C test case..... 25
17. Vibrational temperature contours, RAMM-C test case..... 26
18. Peak electron number density, RAM-C test case..... 26
19. Generic hypersonic vehicle definition..... 27
20. Flight conditions for generic hypersonic vehicle..... 27
21. Computational strategy for hypersonic vehicle flow field... 28
22. Heat transfer at nose section of hypersonic vehicle..... 28
23. Surface mesh of fore body section of hypersonic vehicle.... 29
24. Mesh at symmetry plane of hypersonic vehicle..... 29
25. Pressure contours at symmetry plane of hypersonic vehicle.. 30

26. Velocity vectors at symmetry plane of hypersonic vehicle... 30

27. Surface mesh of hypersonic vehicle..... 31

28. Surface pressure contours of hypersonic vehicle..... 31

29. Heat transfer contours of hypersonic vehicle..... 32

30. Thrust, lift, drag and heat transfer for hypersonic vehicle 32

31(a). Section mesh sizes and time steps to convergence for numerical solution of flow past a generic hypersonic vehicle in powered flight..... 33

31(b). Computational cost of numerical solution for flow past a generic hypersonic vehicle in powered flight..... 33

INTRODUCTION

The development of computational fluid dynamics (CFD) procedures has progressed extremely rapidly during the past two decades. The parallel rapid development in computer hardware resources and architectures has not only matched the explosive algorithm development but has indeed provided and continues to provide its impetus. Together, the resources are now available for the numerical simulation of the flow about complex three dimensional aerospace configurations.

A particularly large growth has occurred during the last few years in the computer hardware sector of scientific workstations. Many vendors are supplying fairly advanced systems for under twenty thousand dollars. Is such a workstation sufficient for solving for the compressible viscous flow about a complete aerospace configuration, perhaps representing a leveling of the playing field previously reserved for those with access to supercomputers? Memory capabilities appear to be expanding rapidly, faster apparently than comparable improvements in hardware speed. The efficiency of the new numerical algorithms may be the deciding factor in answering the above question, at least for the near future.

In reality, the workstation will not replace the supercomputer. However, many of the tasks now performed on supercomputers, such as the important task of program development, can be down shifted to workstations. The tasks of large number crunching can be left to the more powerful supercomputers. In computational fluid dynamics, program development requires many runs of a developing computer code. In three dimensions, even on coarse grids, these runs can be long enough to require the use of a supercomputer. Efficient algorithm development toward faster flow solvers is shortening the durations of these test runs so that in time more and more of them can be made on inexpensive workstations.

Hypersonic flow has been an area of much scientific interest in recent years. The description of a gas flowing about a body traveling at hypersonic speeds is very complex. It must include finite rate chemical reactions as the freestream gas dissociates upon passing through the very strong bow shock wave. Also, because these changes of state occur so rapidly, the gas can be expected to be in thermal nonequilibrium, requiring the determination of separate translational, rotational and vibrational temperatures of the gas. These two additional gas features, chemical reaction and thermal nonequilibrium, require the solution of many additional equations. A perfect gas description in three dimensions requires one continuity equation, three momentum equations and a single energy equation. On the other hand, a nonequilibrium gas requires a continuity equation for each species present, three momentum

equations plus an energy equation for each thermal mode present. For a seven species model for air (N_2,O_2,NO,NO^+,N,O,e^-) and a three temperature gas model (T,Tr,Tvib), thirteen equations are required as compared to five for a perfect gas. Because the gas description is very much more complicated for hypersonic flow, the efficiency of the numerical solution method is of high importance.

The main purpose of the report is to present an efficient numerical method for solving the equations of viscous compressible flow in three dimensions. A main goal of the present study was to apply this method to simulate the flow about a generic hypersonic vehicle in powered flight. This is a rather monumental task that requires very high numerical efficiency to make the calculation possible. The method presented herein is fully implicit and uses block tridiagonal line inversion with Gauss-Seidel relaxation. The block tridiagonal procedure requires the use of a structured grid. This type of algorithm has been very successful in two dimensions where the line direction extended from the body, through the boundary layer fine grid, across the shock wave and into the freestream and where the streamwise direction was treated in a Gauss-Seidel manner. This numerical procedure typically converges for steady-state solutions in under 100-time steps instead of the usual several hundred or thousands for viscous compressible flow simulations. The extension to three-dimensions has proved to be difficult. To avoid a directional bias, a block tridiagonal line inversion procedure is required in the spanwise direction as well. The stitching together of two-line inversion procedures with Gauss-Seidel relaxation to form a numerical method of comparable efficiency to the two-dimensional method will be presented.

A computer program based upon this method has been coded. The computer code has not been vectorized. It has been run only on a serial processing workstation. In addition, for developmental purposes, the program has been written so that Jacobians, for example, have been written as subroutines and called repeatedly by other parts of code. This is less efficient than placing them where needed within the code, but, on the other hand, modifications to the code need to be made only at one place. Furthermore, the Jacobians of the flux vectors in each coordinate direction ($\delta F/\delta U$, $\delta G/\delta U$ and $\delta H/\delta U$ etc.) have been written as a single generalized Jacobian with rotational direction cosines that can be used to determine each individual coordinate direction Jacobian. Again, Jacobian code modifications using this formulation require changes in only one place in the computer program. For the computational efficiency of production runs, unlike code developmental runs, this formulation should be removed and the resulting code should be vectorized to the fullest degree possible.

The computer code was applied to two test-flow problems for which experimental or flight data was available for program validation. The first case simulated the experiment of Lobb [1], 1964, for Mach 15.3 flow past a sphere in air which exhibited

chemical nonequilibrium and thermal vibrational nonequilibrium behavior. The second test case simulated the RAM-C II flight measurements [2] made in the late 1960's of peak electron number densities in the Mach 25.9 flow past a sphere cone body at 71 km. altitude. This flow exhibited ionization and translational, rotational and vibrational nonequilibrium. Finally, the computer program was applied to simulate the flow about a generic hypersonic vehicle at Mach 25 at high altitude. The body consisted of a sphere-cone-cylinder fuselage with a delta wing attached. The delta wing tips were folded up to resemble a hypersonic glider. An engine was then placed below and attached to the fuselage-wing surface. The underside of the body downstream of the engine exit was contoured to form a nozzle surface. The flow entering the engine inlet plane was accelerated to produce thrust at the exit plane. Body drag, engine ram drag, engine thrust and surface heat transfer were calculated.

The present study combines the PhD thesis research on hypersonic nonequilibrium flow of three former Stanford University graduate students, Dr. Graham V. Candler (1988) [3], Dr. Tahir Gokcen (1989) [4], and Dr. Xiao-lin Zhong (1991) [5] with the three dimensional algorithm research presented in Refs. [6,7] to study three-dimensional nonequilibrium hypersonic viscous flow.

GOVERNING EQUATIONS

The Equations governing nonequilibrium viscous compressible flow can be written in vector form as:

$$\frac{\partial U}{\partial t}+\frac{\partial F}{\partial x}+\frac{\partial G}{\partial y}+\frac{\partial H}{\partial z}=W,$$

where $U=[\rho_1,\rho_2,\ldots,\rho_{nr},\rho u,\rho v,\rho w,e_1,\ldots,e_{ne}]^T$, F,G, and H are flux vectors, and W is a source term vector. The flux vectors contain terms representing the convection of species mass, momentum and energy, pressure and viscous stress, work and heat transfer. The viscous and heat transfer coefficients are obtained from Blottner,s curve fits [8] and use of Eucken's [9] and Wilke's relations [10]. The source vector W contains terms for the production and loss of specie densities through chemical reaction and energy transfer through thermal relaxation. Vibrational relaxation is modeled using Park's modified Landau-Teller rate equation [3] and rotational relaxation is modeled using Parker's formulation for relaxation times [11]. Expressions relating vibrational energies to vibrational temperature and energies contained in excited electron states were taken from Candler [3].

The air chemistry model as obtained from Candler's PhD thesis [3] is given below (see top of next page).

$$
\begin{array}{lcllcllcl}
N_2 & + & M & \rightleftarrows & 2N & + & M & & \\
O_2 & + & M & \rightleftarrows & 2O & + & M & & \\
NO & + & M & \rightleftarrows & N & + & O & + & M \\
N_2 & + & O & \rightleftarrows & NO & + & N & & \\
NO & + & O & \rightleftarrows & O_2 & + & N_2 & & \\
N & + & O & \rightleftarrows & NO^+ & + & e^- & &
\end{array}
$$

NUMERICAL METHOD

Chakravarthy in 1984 [12] presented unfactored implicit relaxation methods for solving the Euler equations. By avoiding the technique of approximate factoring and the error it introduces that slows convergence, his approach is very efficient for solving the equations of compressible fluid flow. The approach uses type dependent differencing and line relaxation. These are essentially the same techniques used earlier by Murman and Cole [13] for solving the transonic small disturbance equation and later in rotated form by Jameson [14] for the full potential equation. The type dependent differencing for the Euler equations can use "flux vector splitting" introduced by Steger and Warming [15] or now the more popular "flux difference vector splitting" of Roe [16]. The line relaxation consists of block tridiagonal matrix inversions in the across the flow direction with Gauss-Seidel relaxation used in the streamwise direction. The type dependent differencing is upwind and creates implicit block matrix equations with stronger weights given to the diagonal matrix elements than would otherwise occur using central difference approximations. This facilitates the use of an unfactored relaxation algorithm for the solution of the matrix equation instead of the more common direct approximate factorization algorithm or direct Gaussian elimination with their inherent numerical inefficiencies.

In 1985 efficient Gauss-Seidel line relaxation algorithms for solving the Navier-Stokes equations in two dimensions were presented [17,18]. Their accuracy was improved for calculating laminar and turbulent shear layers in 1987 [19]. Accurate two-dimensional Navier-Stokes calculations were obtained in 100-time steps or less with CFL numbers reaching one billion. Also in 1987, Candler extended the technique to three dimensions for flow past aircraft-like configurations [20]. Block tridiagonal line inversion was used in the normal to the body direction and Gauss-Seidel relaxation in the streamwise and around the body directions. In 1988 difficulties with this method were encountered for three-dimensional cascade flow [6]. Flows that should remain two-dimensional became three-dimensional because the Gauss-Seidel procedure of using the latest available data introduced an asymmetry as each plane was updated using new data on one side and

older data on the other side of the block tridiagonal "line". In addition, the cascade flow required block tridiagonal inversion procedures in both cross stream directions, blade to blade and side wall to side wall. The construction of a three-dimensional unfactored algorithm containing block tridiagonal inversion in two directions is not trivial. The statement found in many algorithm development papers, including this author's, "the extension to three dimensions is straight forward" is untrue.

The three-dimensional implicit algorithm used for the results presented later does combine block tridiagonal inversion in two directions with Gauss-Seidel relaxation in the third direction. It is first order accurate in time and second or third order accurate in space. It could be made second order in time also, but for the problems considered here, for which rapid convergence to steady state was the goal, order of accuracy in time loses its meaning. The governing Navier-Stokes equations with nonequilibrium effects were approximated using low dissipation flux split approximations for the Euler terms as described in Ref. [19] and central difference approximations for the viscous terms.

Consider the flux at surface i+1/2 lying midway between mesh points (i,j,k) and (i+1,j,k). The flux F can be split as follows.

$$F_{i+1/2,j,k} = A^{+}_{i+1/2} U_L + A^{-}_{i+1/2} U_R$$

where A is the Jacobian $\delta F/\delta U$, A^{+} and A^{-} represent the split Jacobians containing the positive and negative eigenvalues, respectively, of A, and $A = A^{+} + A^{-}$. U_L represents the value of U at the surface as approached from the left, and U_R is similarly defined using data from the right. At flux surfaces that are supersonic on both sides the flux is not split at all; either A^{+} or A^{-} is null. At surfaces within subsonic regions of the flow and away from shock waves third order flux splitting is achieved by (1) using an interpolation formula and the nearest four points, (i-1,j,k), (i,j,k), (i+1,j,k) and (i+2,j,k), to define the elements of the split flux Jacobian matrices, and (2) using interpolation with three upwind biased points, (i-1,j,k), (i,j,k) and (i+1,j,k), to define U_L and similarly using points (i,j,k), (i+1,j,k) and (i+2,j,k) to define U_R. The third order approximations are important within boundary layers to prevent the numerical dissipation introduced by the flux splitting from significantly competing with viscous terms of the governing differential equations. Through reflective boundary conditions, third order differencing can be carried all the way to the wall. Finally, at shock waves, where pressure gradients are large, and the flow is supersonic on one side of surface i+1/2 and subsonic on the other, first order flux splitting is used.

For each mesh point in a three-dimensional flow the algorithm uses data from 24 four neighboring points to evaluate all the spacial derivatives of the full Navier-Stokes equations explicitly.

This is used to construct the explicit driving term, sometimes called the residual term, on the right hand side of the difference equations. The left hand implicit side of the difference equations uses data at only six mesh points plus the central point itself. Only the thin layer Navier-Stokes terms are evaluated implicitly. The mesh points are located at the centroids of finite volumes forming the discretized space surrounding the body. The resulting block seven-diagonal matrix equation is formulated in delta law form. That is, the solution change per time step, δU, is the unknown to be solved for. The matrix equation is given below.

$$\hat{A}\delta U_{i,j,k}+\hat{B}\delta U_{i,j+1,k}+\hat{C}\delta U_{i,j-1,k}+$$

$$\hat{D}\delta U_{i+1,j,k}+\hat{E}\delta U_{i-1,j,k}+$$

$$\hat{F}\delta U_{i,j,k+1}+\hat{G}\delta U_{i,j,k-1}= \Delta U_{i,j,k}$$

$$where$$

$$\Delta U_{i,j,k}=-\Delta t\left(\frac{DF}{\Delta x}+\frac{DG}{\Delta y}+\frac{DH}{\Delta z}-W\right)^{n}_{i,j,k}$$

The hepta-diagonal matrix equation is inverted by relaxation as follows. The mesh points are ordered into an i,j,k array. The values for the unknown δUs are initialized by setting them to zero. For each i plane a block tridiagonal inversion in the j direction is carried out for each value of k in the plane. During this inversion, evaluations needed at points (i+1,j,k) and (i-1,j,k) adjacent to a line of constant i,k use the latest available data in line Gauss-Seidel fashion. Evaluations needed at off line points (i,j,k+1) and (i,j,k-1) may use data from the last block tridiagonal inversion along the line of constant i,j, if it exists, in line Jacobi fashion. Yet, in the present code an axisymmetric approximation for these terms is used instead. This approximation effectively replaces these two terms at (i,j,k+1) and (i,j,k-1) with a new one at the diagonal element (i,j,k). This first step procedure is shown below (see top of the next page). In the equation for this procedure the δUs at (i,j+1.k), (i,j,k) and (i,j-1,k) are solved for simultaneously.

After completion of the first step, block tridiagonal inversion in the k direction proceeds for each j in the i plane. As before, evaluations at (i+1,j,k) and (i-1,j,k) are made in line Gauss-Seidel fashion and those at (i,j+1,k) and (i,j-1,k) are also made in Gauss-Seidel fashion. It was found that it was best to order these k-direction block tridiagonal inversions from the top down, that is, in the descending j direction. Thus, the newest information is moving in the same direction as the principal

GAUSS-SEIDEL LINE RELAXATION - STEP 1
BLOCK TRIDIAGONAL INVERSION - j DIR.

$$\hat{A}\delta U^{(m)}_{i,j,k}+\hat{B}\delta U^{(m)}_{i,j+1,k}+\hat{C}\delta U^{(m)}_{i,j-1,k}+$$

$$\hat{D}\delta U^{(*)}_{i+1,j,k}+\hat{E}\delta U^{(*)}_{i-1,j,k}+$$

$$\hat{F}\delta U^{(\hat{*})}_{i,j,k+1}+\hat{G}\delta U^{(\hat{*})}_{i,j,k-1}= \quad \Delta U_{i,j,k}$$

(*) *indicates latest available data*
($\hat{*}$) *indicates axisymmetric approximation*

component of the flow in the i plane, from the freestream, through the bow shock wave and toward the body. Therefore, the data for δU at (i,j+1,k) comes from the last k-direction line inversion at j+1 and that for (i,j-1,k) comes from a j-direction line inversion from step 1. This second step is given below.

GAUSS-SEIDEL LINE RELAXATION - STEP 2
BLOCK TRIDIAGONAL INVERSION - k DIR.

$$\hat{A}\delta U^{(m+1)}_{i,j,k}+\hat{B}\delta U^{(m+1)}_{i,j+1,k}+\hat{C}\delta U^{(m)}_{i,j-1,k}+$$

$$\hat{D}\delta U^{(*)}_{i+1,j,k}+\hat{E}\delta U^{(*)}_{i-1,j,k}+$$

$$\hat{F}\delta U^{(m+1)}_{i,j,k+1}+\hat{G}\delta U^{(m+1)}_{i,j,k-1}= \quad \Delta U_{i,j,k}$$

(*) *indicates latest available data*

After the inversion procedures for both the j and k directions within plane i have been completed the next i plane is processed. In general, each i plane is processed from the last to the first and then a second time from the first back to the last. However, if the flow is supersonic in the i-direction, or more precisely, if the flow component normal to each i plane is supersonic at each mesh point in the flow, except within the boundary layer region, then only one sweep needs be made from the inlet i-plane to the exit i-plane. The algorithm requires one block tridiagonal inversion for each i,j and i,k line in the mesh per sweep per time step. It is symmetric with respect to the j and k directions but

not the i direction.

DISSIPATION

There is no added dissipation in the present method. But this does not mean that there is no dissipation in the numerical method. All methods require numerical dissipation to control numerical instabilities. It is an essential ingredient. The present method contains dissipation through the upwind flux split difference approximations to the Euler terms plus the centered difference approximations used for the viscous terms only. Dissipation introduced this way is said to be genuine. When dissipation is introduced by adding new terms to the difference equations that do not correspond to terms in the governing differential equations, it is artificial. Some justify the latter kind because they are able to control the amount added by turning up or down a parameter multiplying the added term. It can be turned up to the point of rendering a hyper-active numerical solution comatose, perhaps masking the effect of a fundamental bug in the program. If something is wrong in the program, it is better to have a quick death than a lingering program life. In general, humans can not be trusted with artificial viscosity in numerical calculations.

Yet dissipation is essential. The successes of computational fluid dynamics can be explained in terms of the numerical methods having the right dissipation. Many tried unsuccessfully to solve the transonic small disturbance equation using central differences at each mesh point before Murman and Cole [13] made the modification to use backward differences in supersonic flow regions. Central differences at supersonic flow mesh points are anti-dissipative and backward differences are dissipative. Many rushed to use this strategy on the full potential equation without success until Jameson [14] devised a rotated difference scheme that again had the effect of replacing anti-dissipative difference approximations with dissipative ones. Neither case had terms added artificially to the difference equations.

The Steger-Warming flux vector split procedure is fairly dissipative, too dissipative to be used where viscous effects are important. It was originally intended to be used to solve the inviscid Euler equations, but it can be modified to greatly reduce its dissipation so that it can be used for viscous flow as well. The Roe flux difference vector splitting procedure can also be used for viscous flow as it is, but under certain flow conditions additional dissipation, sometimes called entropy correction, needs to be added. The method of the present paper uses a modified version of the Steger-Warming procedure described in Ref.[19]. It is used throughout the flow field in both viscous and inviscid flow regions. However, it is not always sufficient to control numerical difficulties and in some regions of the flow the original more dissipative Steger-Warming procedure is blended in with it. These

difficulties occur at shock waves.

DIFFICULTIES AT SHOCKS

The numerical difficulties at shock waves can be categorized as either annoying or catastrophic. The annoying consist of numerical shock buzz, which is the continual moving of the shock forward and backwards without ever settling down. This motion can be either periodic or a chaotic non-repeating motion. When it is present it occurs near the stagnation streamline of the flow. It feeds on a supersonic-subsonic interaction at the bow shock wave. The catastrophic consist of negative temperatures and densities occurring at the foot of the shock, also usually located near the stagnation streamline. These difficulties are magnified as the CFL number is increased. For this study CFL numbers of the order of one million were used. The workstation word size essentially limited the CFL to this value, not the numerical method.

The alignment of the grid with the shock near the stagnation streamline is a key factor in producing or eliminating these difficulties. Perfect alignment along the entire shock is impractical unless the mesh is actively shock-fit during the calculation. It was observed that where errors in the alignment occur, it was better for the shock to cut through the mesh toward the body rather than toward the freestream. This tends to reduce the feedback or interaction mechanism within the subsonic region behind the strong part of the bow shock.

Secondly, as mentioned above, pure Steger-Warming was blended in with modified Steger-Warming flux splitting at shock wave locations. The amount used depended upon the pressure gradient, PG. The weight function used for it varied from zero to one according to the formula

$$WT = 1.0-1.0/(1.0+PG*PG)$$

Analysis of the Steger-Warming algorithm shows that there is a considerable mixing of fluid across mesh surfaces. This should lead to a smearing of the shock that prevents negative densities and temperatures. This is exactly what occurs when it is used explicitly. Densities and energies, both positive quantities, are mixed. However, when it is also used implicitly as in the delta law form of the difference equations given above, it mixes the "changes" in densities and energies. These changes can be of either sign. Negative changes can be mixed forward through the shock wave causing negative densities and energies in the freestream at the foot of the shock. To avoid this from happening, the blending in of pure Steger-Warming was used only to obtain the explicit $\Delta U_{i,j,k}$ in the above equations and was not used at all on the implicit side, the left side, of the block matrix equations given above.

STABILITY

The present numerical technique is implicit and can be run with CFL numbers as high as a billion. Yet, a calculation cannot be started with any arbitrarily large time step size. Initially the transients in the solution are large and, even though the method may be stable according to linear theory for any time step size, it is limited in practice because of the non-linearity of the governing equations being solved. One would expect this if the Jacobian matrices appearing on the implicit side of the approximating finite difference equations, or as in the present case finite volume equations, change significantly during a single time step. In impulsively started viscous flow calculations, exceptionally high shear exists at no slip boundary surfaces. Large transients can also occur in the flow field after the start of the calculation, perhaps associated with the movement of a strong bow shock wave. In a large three-dimensional calculation it is difficult to anticipate all such transients and then to determine how large the time step can be a priori. Each calculation can represent a significant investment in computer time which can be lost if it becomes unstable.

To avoid this difficulty, a new subroutine was built into the present three-dimensional Navier-Stokes program to automatically adjust the time step through periods of strong flow transients. A time step is chosen initially rather arbitrarily and increased geometrically during the calculation. At each time step, after the changes in the solution have been computed implicitly, the changes are checked to determine if either density at any mesh point in the flow will change by more than a factor of one-half, or if an internal energy any where in the flow field will decrease by more than a factor of one-half. If either condition is true, the time step during that step is cut to that value for which either the density or internal energy will be limited to a change of at most half. The solution changes do not have to be recalculated implicitly because they depend linearly on the time step size. They need only to be cut everywhere by the same factor the time step is cut. An alternative version of cutting the time step locally was tried with some success also, but it introduces non-conservation into the calculation which was not preferred. For the computed results to be presented, reductions in time step size were observed periodically during the early part of the calculations, but then the need for time step reductions disappeared entirely as convergence occurred. In addition, the time step was increased continuously during the calculation at a rate that doubled it every eight steps.

COMPUTATIONAL RESULTS

The computer code was applied to two test flow problems for

which experimental or flight data was available for program validation.

Lobb Test Case

The first case simulated the experiment of Lobb in 1964 [1] for Mach 15.3 flow past a sphere of radius 0.635cm. and Reynolds number 1.47×10^4 in air. The freestream pressure was 664 Newtons per square meter, the freestream temperature was 293K and the body surface temperature was fixed at 1000K. The shock wave position was guessed at the start of the calculation and inviscid shock wave theory was used to define the initial solution. Two cases were run, perfect gas and seven species reacting air, on an axisymmetric 24x30 mesh shown in Fig.1. Care was taken to fit the mesh to the shock near the axis of symmetry. The shock wave locations for each case are shown in Fig.2 compared with the experimental data of Lobb obtained from a Schlieren photograph. The shock wave represents in a sense the integrated effect of the state of the gas between the body and shock. Note the nonequilibrium results compare much better with the experimental results, indicating significant nonequilibrium flow is present. Both Candler [3] and Gokcen [4] used this test case for code validation with excellent agreement with experiment. Notice the shock ripples near the exit as the shock crosses through the mesh. Although the shock simulation is degraded in this region, it did not cause any of the difficulties discussed earlier because it occurred downstream of the sonic line.

The pressure contours for nonequilibrium flow are shown in Fig.3 and mass fractions for specie NO are shown in Fig.4 Note that the NO mass fractions concentrate in a region between the body and shock. The mass fractions of NO are zero in the freestream, build up upon passing through the shock wave where dissociated nitrogen and oxygen are found and then decrease as NO dissociates in the wall cooled boundary layer. The wall was assumed to be noncatalytic. The stagnation streamline temperatures are shown in Fig.5. In the figure the body is located at x=0 and the shock approximately x/r=-0.085. Note that the rotational temperature is in equilibrium with the translational temperature everywhere except near the shock, and the vibrational temperature is out of equilibrium everywhere except where the stagnation streamline approaches the body fixed wall temperature of 1000K. Figures 6-8 show contours of translational, rotational, and vibrational temperatures. Note again that the rotational temperature is in equilibrium with the translational temperature almost everywhere and that the vibrational temperature is out of equilibrium almost everywhere. These results agree with those of Candler [3] who assumed rotational equilibrium and with Gokcen [4] who did not.

RAM-C II Flight Measurements

During the late 1960's sphere cone bodies were rocket launched, turned around at high altitudes and fired down through the upper atmosphere [2]. Microwave antenna carried on board the vehicle made measurements of peak electron number densities. This

flow field was simulated numerically by Candler [3] with excellent agreement at all altitudes calculated. In the present study, only one altitude at 71 km will be considered. The sphere-cone body of nose radius 0.1524m, cone half angle of 9° and body length of 1.295m traveled at Mach 25.9 The freestream pressure was 4.898 Newtons per square meter and the freestream temperature was 216K. The body surface was assumed to be noncatalytic and at a fixed 1500K. The axisymmetric 24x30 mesh and pressure contours are shown in Figs. 9 and 10.

The translational, rotational and vibrational temperature profiles along the stagnation streamline are shown in Fig.11. This flow exhibited considerable translational, rotational and vibrational nonequilibrium before arriving at the fixed wall temperature. The shock wave location appears to be approximately x/r=-0.1. Figure 12 shows the mass fractions of N_2, O_2, NO, N and O also along the stagnation streamline. Note that the shock wave appears here to be located at only x/r=-0.07. The difference is explained by the need to build up a significant vibrational temperature before dissociation of N_2 and O_2 can occur as is formulated by Park's geometric mean temperature [3], $(T*T_{vib})^{1/2}$, used in the chemical rate equations. Note also that the species nearly all return to their freestream values at the wall. Although the wall is noncatalytic, it is sufficiently cool to bring about recombination of N_2 and O_2. The contours of N_2 and O_2 are given in Figs. 13 and 14. Note also here that the species return to near their freestream values along the whole length of the body. Figures 15-17 show contours of translational, rotational and vibrational temperatures. Note that although these three temperatures were far out of equilibrium along the stagnation streamline, the rotational temperature is in fairly good agreement, as assumed by Candler [3], for most of the flow field and vibrational temperature remains in nonequilibrium almost everywhere.

Figure 18 compares the measured peak electron number densities with the computation. The flow field was calculated in two parts, the nose section, $x < 2.4$, and the section downstream of the nose, $x > 2.4$. Although this flow could have been calculated on a single mesh, this test served to illustrate the sectional calculation of a supersonic flow field. This is more efficient because no calculations need be made until the flow section immediately ahead is converged. This figure also illustrates the speed of convergence of the present numerical method. After the nose section converged, the data at the nose section exit was used to initialize the flow field of the downstream section. Convergence was then obtained in only about 16 time steps. Note the comparison with the experiment is not perfect, but also note that there is a four decade variation in number densities shown within this figure. The thought of getting as close to the measured values as shown here was only a hope a priori to performing the calculation. For this same altitude of 71 km., Candler [3] fit the data

exceptionally well on a finer grid.

Generic Hypersonic Vehicle

The computer program was applied to simulate the flow about a generic hypersonic vehicle at Mach 25 and at high altitude. The body consisted of a sphere-cone-cylinder with a delta wing attached. The delta wing tips were folded up to resemble a hypersonic glider. An engine was then placed below and attached to the wing-fuselage. The underside of the body downstream of the engine exit was contoured to form a nozzle surface. A side view of the body and its dimensions are given in Fig.19 and flight conditions are given in Fig.20 with a rotated side view of the vehicle. The computational strategy is given in Fig.21 with a view of the underneath side of the vehicle. The flow was cut into four sections, nose, fore body, engine and after body nozzle sections. Because of body and flow symmetry, only the flow on one side of the body symmetry plane needed to be computed. Each section was run in order from the nose to the tail, and only after the preceding section converged. The solution at the exit plane of each section was used to initialize the flow in the section just downstream of itself. If the geometry at the exit resembled the geometry of the neighboring downstream section, as is the case near the nose, this initialization facilitated fairly rapid numerical convergence, otherwise, as at the last section of the body, convergence was slower.

Heat transfer contours on the nose surface are shown in Fig.22. Care must be used in reading values from the key or table at the right side of the figure because the highest values shown in kilowatts per square meter have been divided by 10 by the plotting software. Stagnation point heating is 4.9×10^5 and heating along the leading edge of the emerging wing approaches 2.8×10^5 kilowatts per square meter at the exit of the nose section.

A surface grid for the fore body section is shown in Fig.23 and a cross section of the mesh along the symmetry plane is shown in Fig.24. The mesh has thirty finite volume cells from body to free stream. The flow entering the engine inlet plane was accelerated to produce thrust at the exit plane without changing the mass flow rate. The temperatures of the gas entering the engine inlet was approximately the same as that leaving the engine exit. The flow acceleration was designed to be approximately equal to the sum of the vehicle surface drag and engine ram drag. The flow at each mesh point leaving the fore body mesh and entering the engine inlet was accelerated and mapped one to one with mesh points entering the after body nozzle section from the nozzle exit. Other values at the inlet planes of the engine and after body nozzle sections were obtained by interpolation from the corresponding exit planes. Pressure contours and velocity vectors in the symmetry plane are shown in Figs. 25 and 26. Note the clearly defined laminar boundary layers appearing in the velocity vector plot.

The surface mesh of the generic hypersonic vehicle is shown in Fig.27. The trailing edge of the vehicle is a knife edge as are the engine inlet and exit surfaces. Surface pressure contours in Newtons per square meter are shown in Fig.28. The peak surface pressure occurs at the stagnation point and achieves a value of 4.1×10^3. High surface pressures also occur along the leading edges of the folded delta wing. Surface heat transfer contours are shown in Fig.29 again with peak heating at the nose and wing leading edges. Total thrust, lift, drag and heat transfer for the generic hypersonic vehicle are given in Fig.30. Engine thrust was adjusted to give a net forward impulse to the vehicle.

A summary of the bookkeeping in terms of section mesh sizes and number of time steps to convergence is given in Fig.31. Section 4, the after body nozzle section, took the longest to converge. The flow in this section had the longest way to go from the initial condition to converged solution, because of extreme flow conditions in the expanding nozzle region downstream of the engine exit. The automatic time step reduction procedure, described in the stability section of this paper, was called at each time step during the first 32 time step run, thus reducing the actual flow time simulated. The program was run an additional 64 time steps, the last half of which did not require automatic time step reductions. At approximately 96 time steps, the flow settled out.

The computational cost of this three-dimensional Gauss-Seidel line relaxation method on a mesh of size ILxJLxKL is approximately the time taken by ILx(JL+KL) block tridiagonal inversions. On a SUN SPARCstation 1, a section mesh of 24x31x26, for 32 time steps, integrating the 13 equations governing chemically reacting thermal nonequilibrium flow, required approximately 5 days to finish. The flow field calculation for each section was run in the background while the workstation was used also to set up the mesh and initial conditions required for the next flow section. However, the human times required to set up the surface geometry and mesh for the next section to be done were usually longer than 5 days. Thus, the SPARCstation 1, relatively slow by today's standards, was sitting idle much of the time. Nevertheless, this calculation of the nonequilibrium flow past a complete hypersonic vehicle in powered flight is believed to be the first anywhere, even at aeronautical laboratories with supercomputer access.

CONCLUSION

An efficient numerical method has been presented for solving the compressible Navier-Stokes equations in three dimensions. It has been extended to solve for the chemically reacting flow in thermal nonequilibrium encountered under hypersonic conditions. Experimental and flight test data have been used to validate a computer program based upon this method. The program has been

used, on an inexpensive computer workstation, to predict the complete flow field about a generic hypersonic vehicle in powered flight.

REFERENCES

1. Lobb, R.K., "Experimental Measurement of Shock Detachment Distance on Spheres Fired in Air at Hypervelocities," in The High Temperature Aspects of Hypersonic Flow, ed. W.C. Nelson, Pergammon Press, MacMillan Co., New York, 1964.
2. Jones, W.L. and Cross, A.E., "Electrostatic Probe Measurements of Plasma Parameters for Two Reentry Flight Experiments at 25,000 Feet per Second," NASA TN D-6617, 1972.
3. Candler, G.V., "The Computation of Weakly Ionized Flows in Thermo-Chemical Nonequilibrium," PhD. Thesis, Stanford University, 1988.
4. Gokcen, T., "Computation of Hypersonic Low Density Flows with Thermochemical Nonequilibrium," PhD. Thesis, Stanford University,1989.
5. Zhong, X-1., "Development and Computation of Continuum Higher Order Constitutive Relations for High Altitude Hypersonic Flow," PhD. Thesis, Stanford University, 1991.
6. R.W. MacCormack, "On the Development of Efficient Algorithms for Three Dimensional Fluid Flow," ASME Publication, Recent Developments in Computational Fluid Dynamics, AMD, Vol. 95, 1989.
7. MacCormack, R.W., "Solution of the Navier-Stokes Equations in Three Dimensions," AIAA Paper No. 90-1520, 1990.
8. Blottner, F.G., Johnson, M. and Ellis, M., "Chemically Reacting Viscous Flow Program for Multi-Component Gas Mixtures," Report No. SC-RR-70-754, Sandia Laboratories, Albuquerque, New Mexico, 1971.
9. Vincenti, W.G. and Kruger, C.H.,Jr., "Introduction to Physical Gas Dynamics," Krieger Publishing Company, Florida, 1965.
10. Wilke, C.R., "A Viscosity Equation for Gas Mixtures," J. Chem Phys., 18, pp 517-519, 1950.
11. Parker, J.G., "Rotational and Vibrational Relaxation in Diatomic Gases," Physics of Fluids, 2, 449, 1959.
12. Chakravarthy, S.R., "Relaxation Methods for Unfactored Upwind Schemes," AIAA Paper No. 84-0165, 1984.
13. Murman, E.M., and Cole, J.D., "Calculation of Plane Steady Transonic Flows," AIAA Journal, Vol. (No. 1, January 1971, pp 114-121.
14. A. Jameson, "Numerical Calculation of the Three dimensional Transonic Flow Over a Yawed Wing," Proceedings, AIAA Computational Fluid Dynamics Conference, Palm Springs, CA, July 19-20, 1973.
15. J.L. Steger and R.F. Warming, "Flux Vector Splitting of the Inviscid Gasdynamic Equations with Application to Finite Difference Methods," Jour. Comp. Phys., Vol.40, No.2, pp.263-293, 1981.
16. P.L. Roe, "Characteristics-Based Schemes for the Euler Equations," Ann. Rev. Fluid. Mech., Vol.18, pp 337-365, 1986.
17. J.L. Thomas and R.W. Walters, "Upwind Relaxation Algorithms for the Navier-Stokes Equations," AIAA Paper No. 85-1501, 1985.

18. R.W. MacCormack, "Current Status of Numerical Solutions of the Navier-Stokes Equations," AIAA Paper No. 85-0032, 1985.
19. R.W. MacCormack and G.V. Candler, "The Solution of the Navier-Stokes Equations Using Gauss-Seidel Line Relaxation," Computers and Fluids, Vol. 17, No. 1, pp 135-150, 1989.
20. G.V. Candler and R.W. MacCormack, "Hypersonic Flows Past 3-D Configurations," AIAA Paper No. 87-0480, 1987.

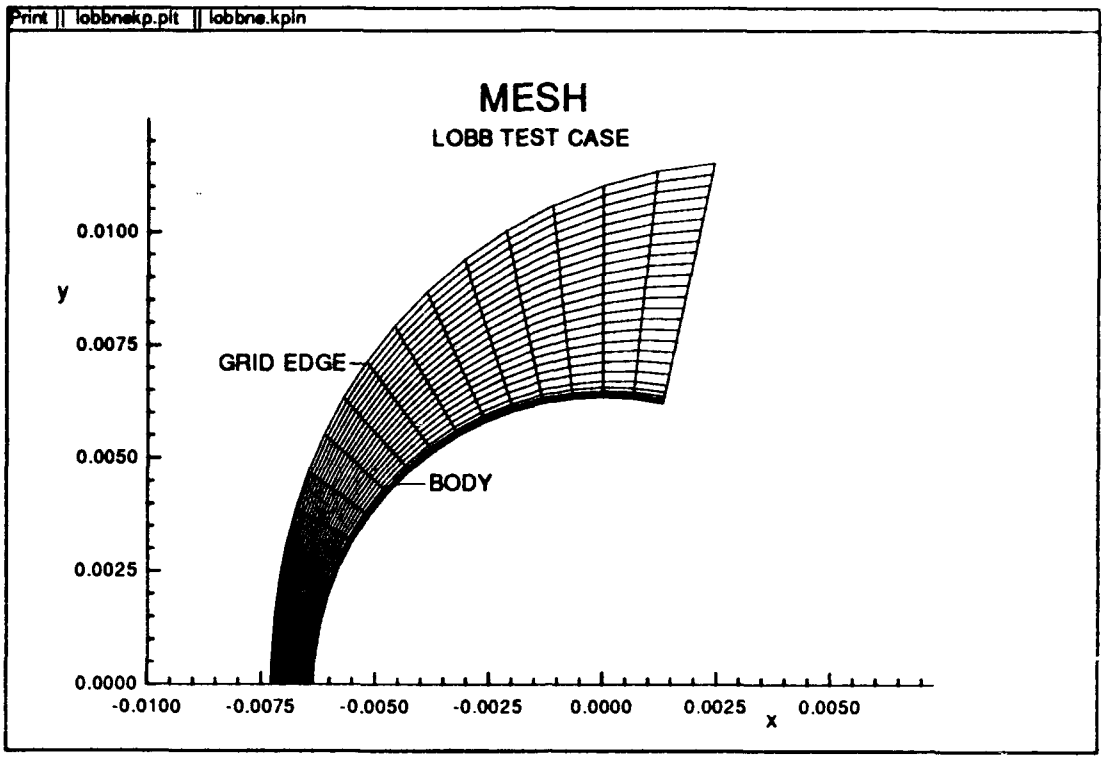

Fig.1 Computational mesh for Lobb test case.

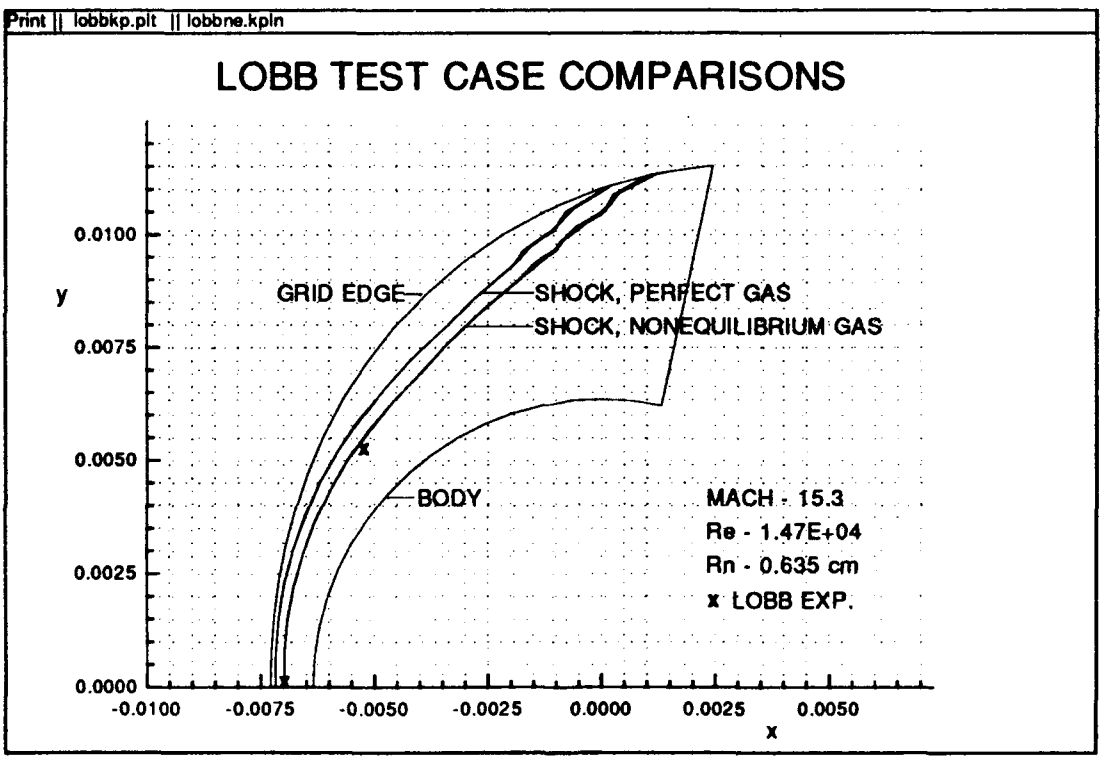

Fig.2 Comparison of shock wave locations, Lobb test case.

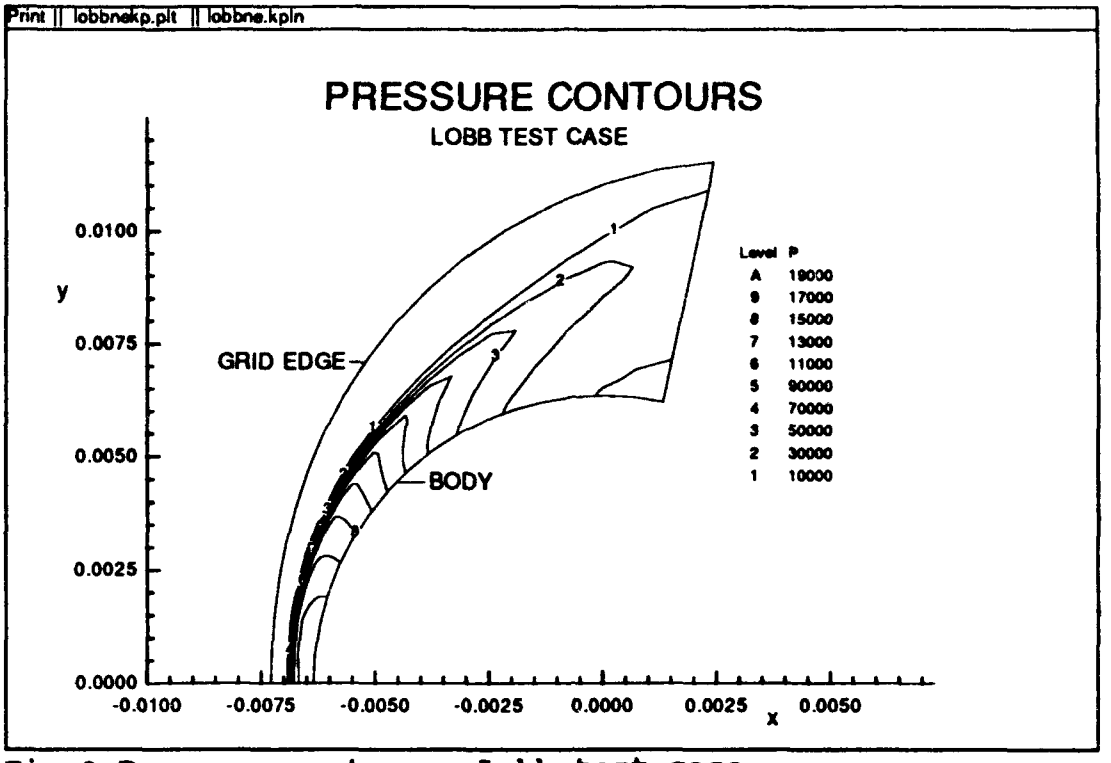

Fig.3 Pressure contours, Lobb test case.

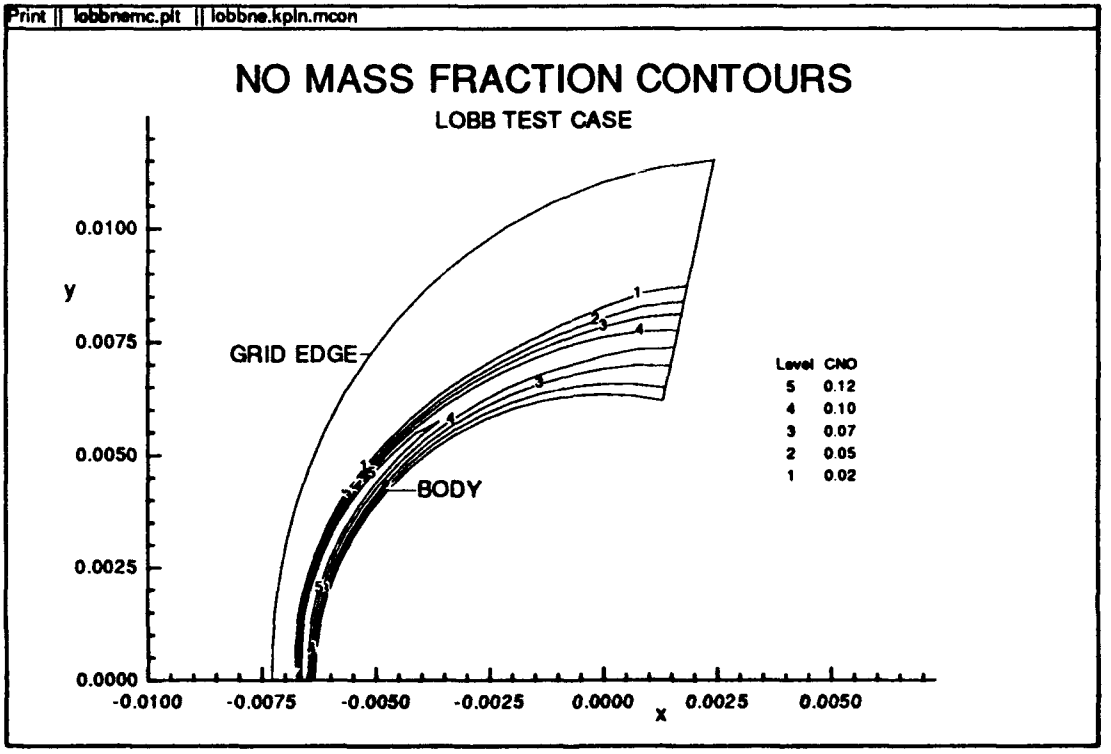

Fig.4 NO mass fractions, Lobb test case.

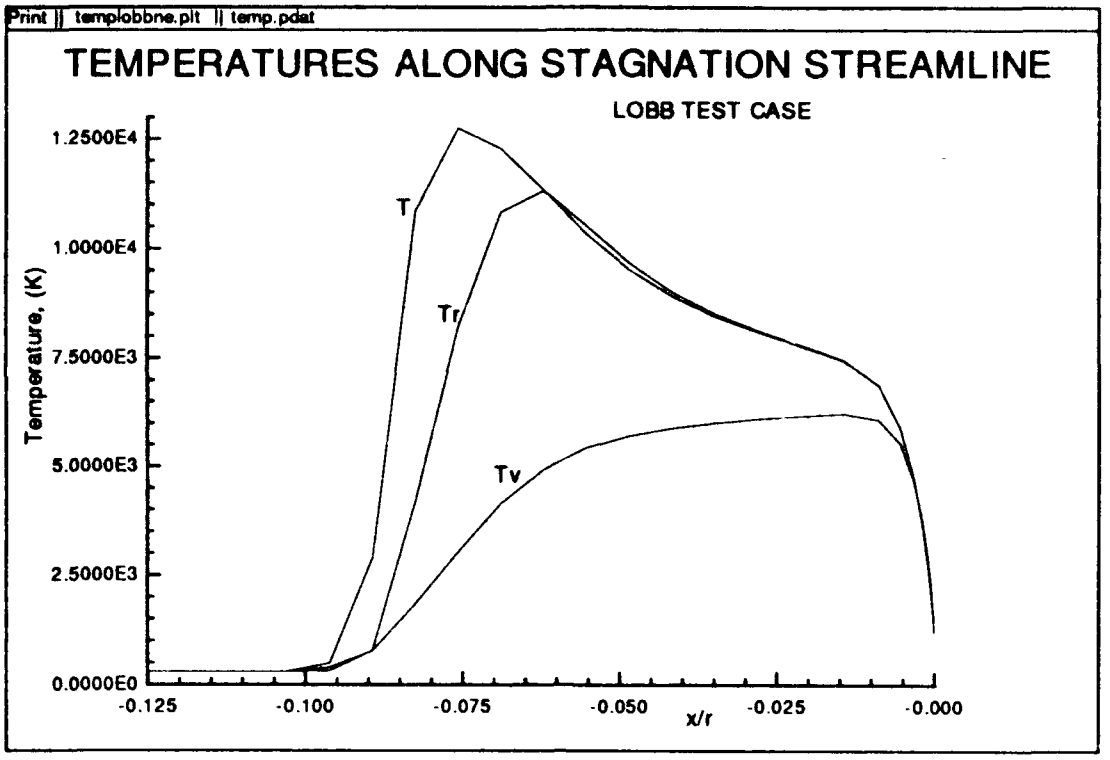

Fig.5 Stagnation streamline temperature profiles, Lobb test case.

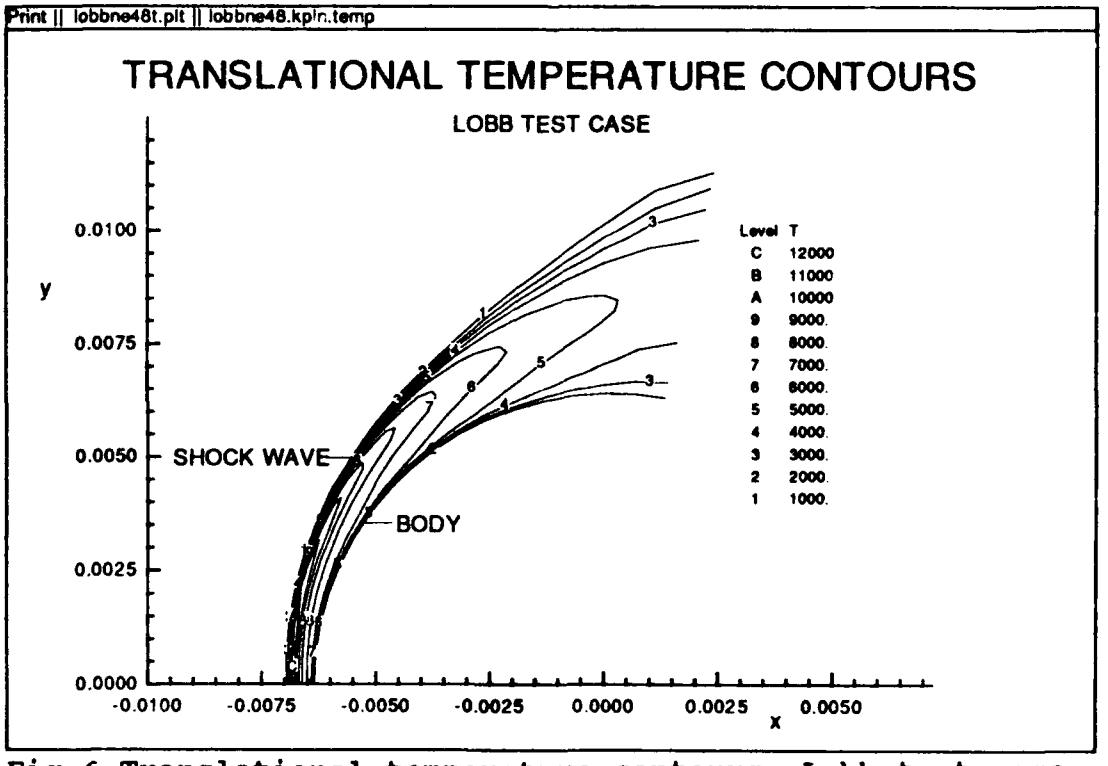

Fig.6 Translational temperature contours, Lobb test case.

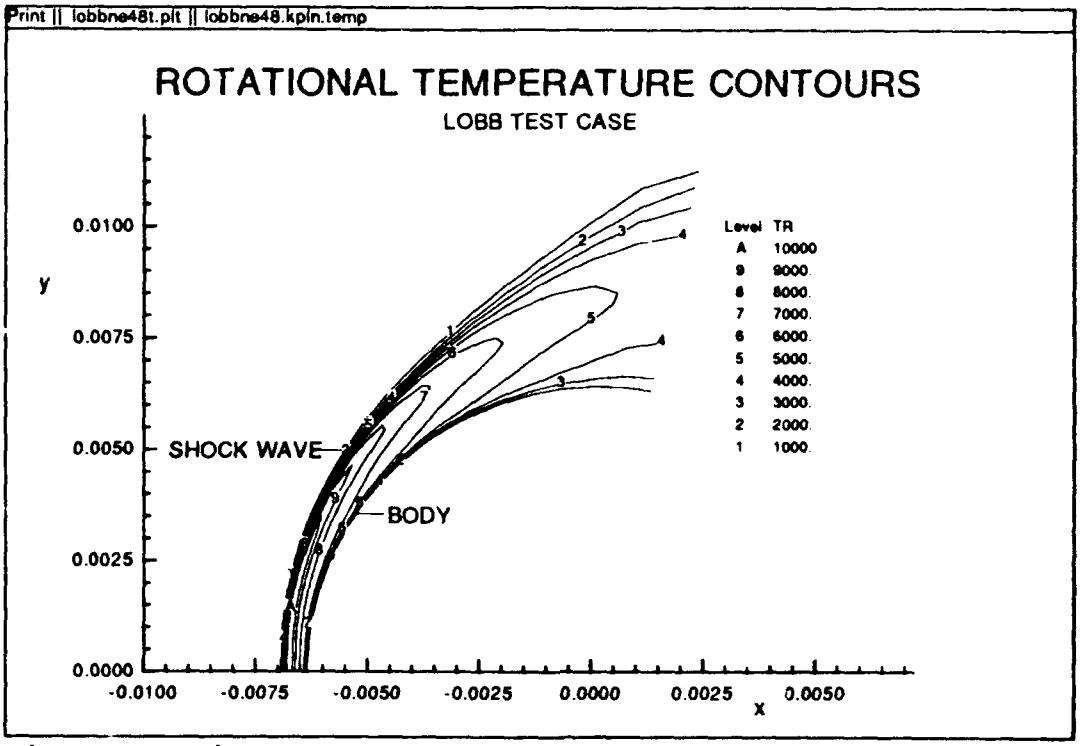

Fig.7 Rotational temperature contours, Lobb test case.

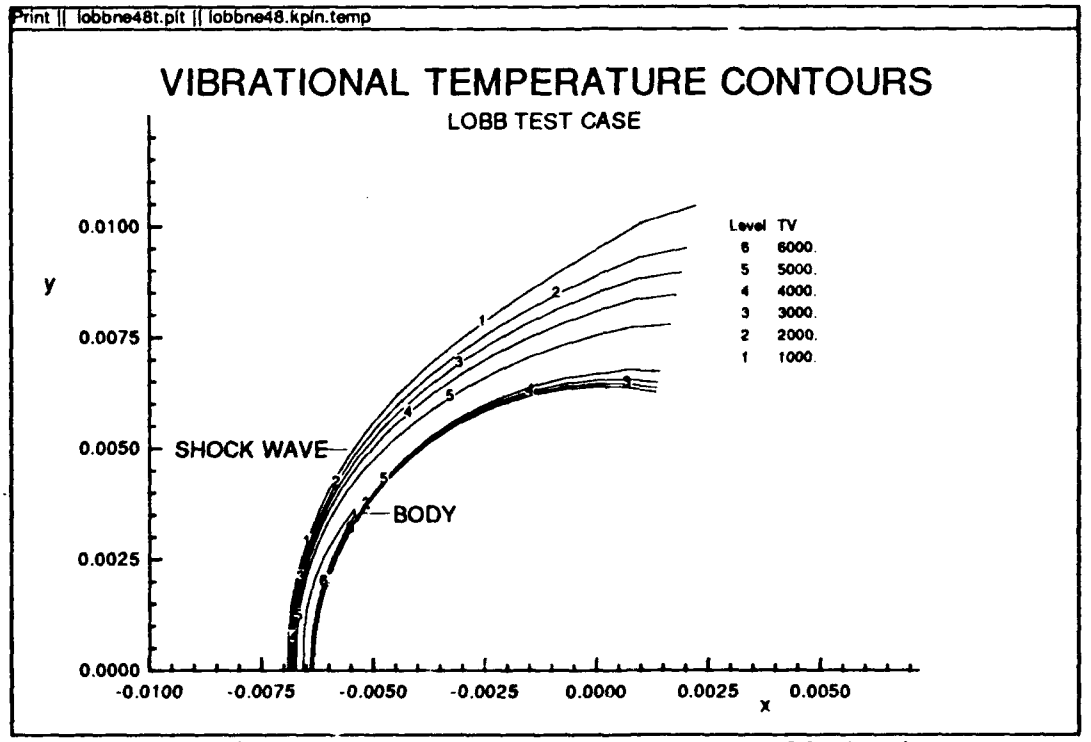

Fig.8 Vibrational temperature contours, Lobb test case.

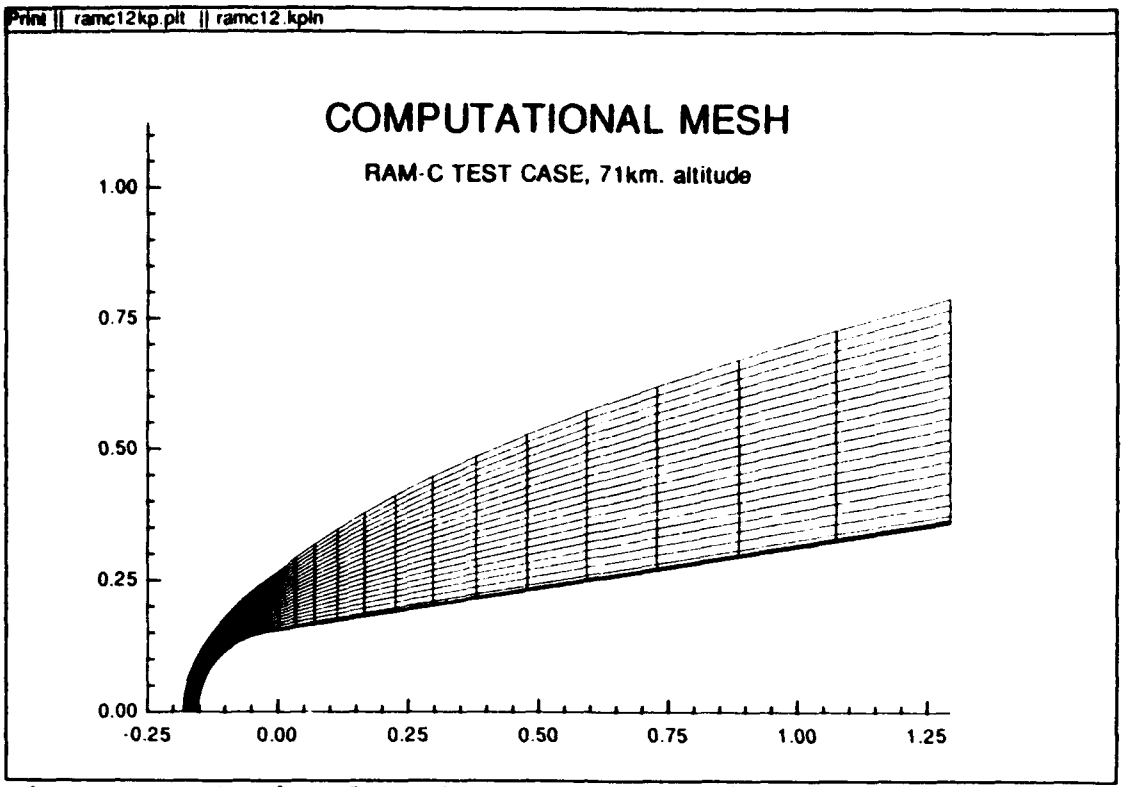

Fig.9 Computational Mesh, RAM-C II test case.

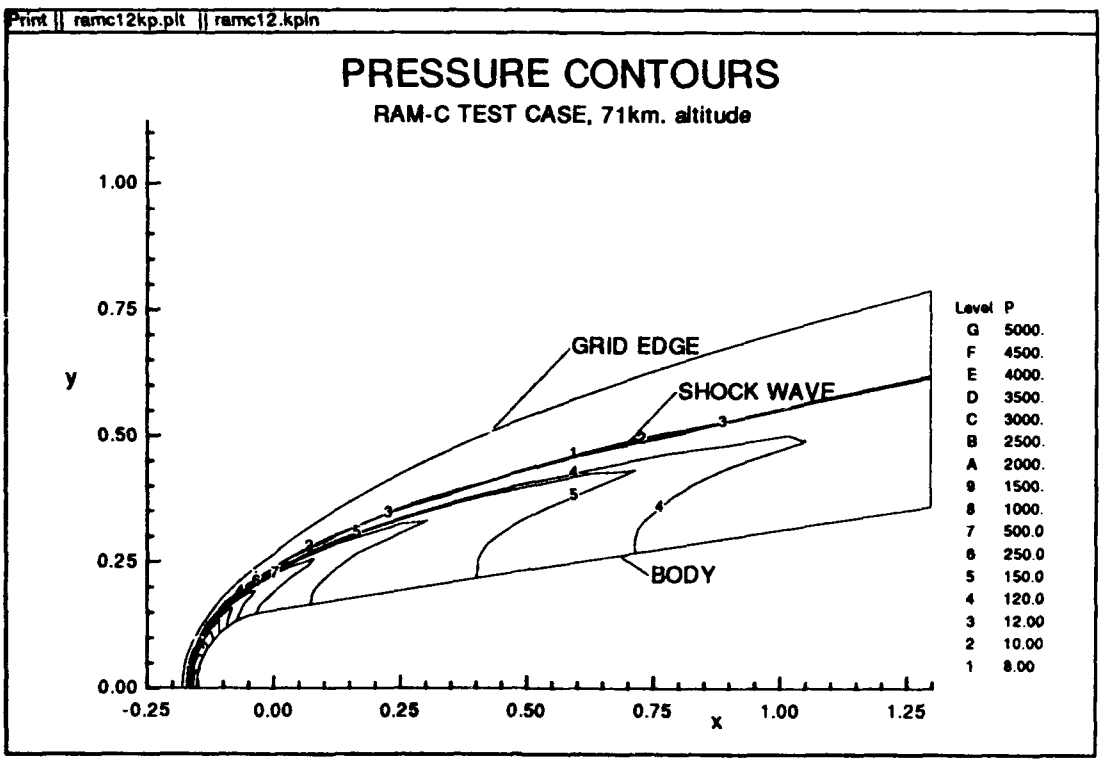

Fig.10 Pressure contours, RAM-C II test case.

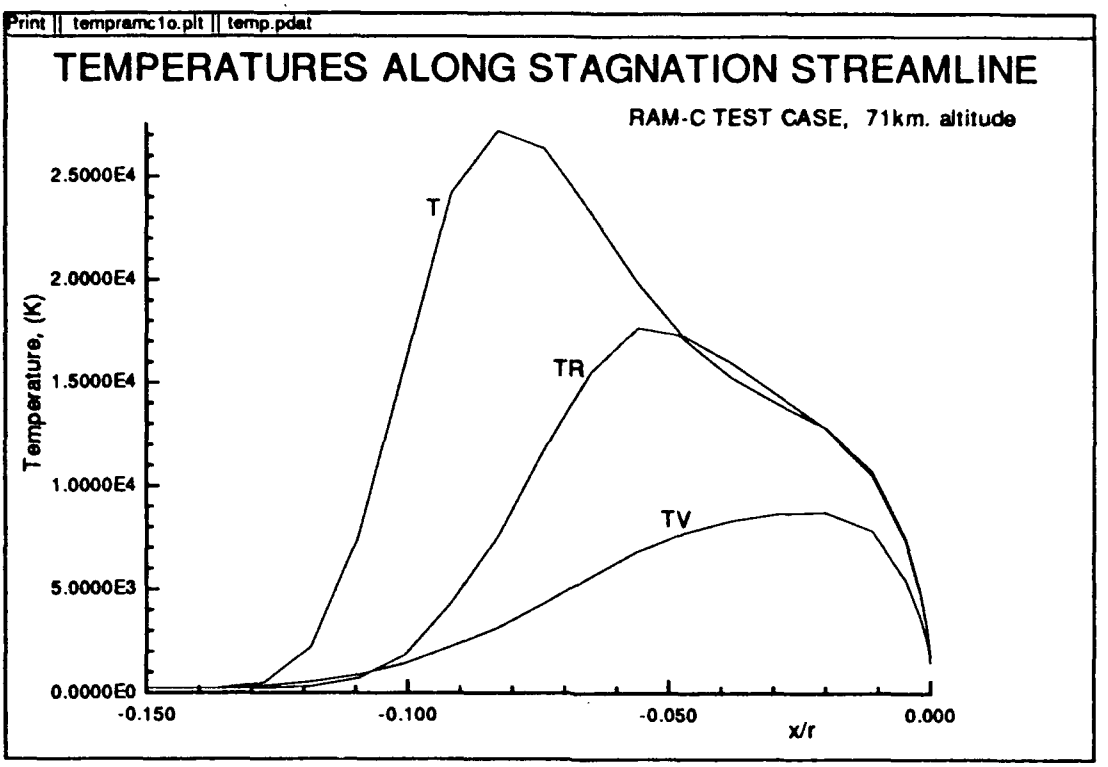

Fig.11 Stagnation streamline temperature profiles, RAM-C II test case.

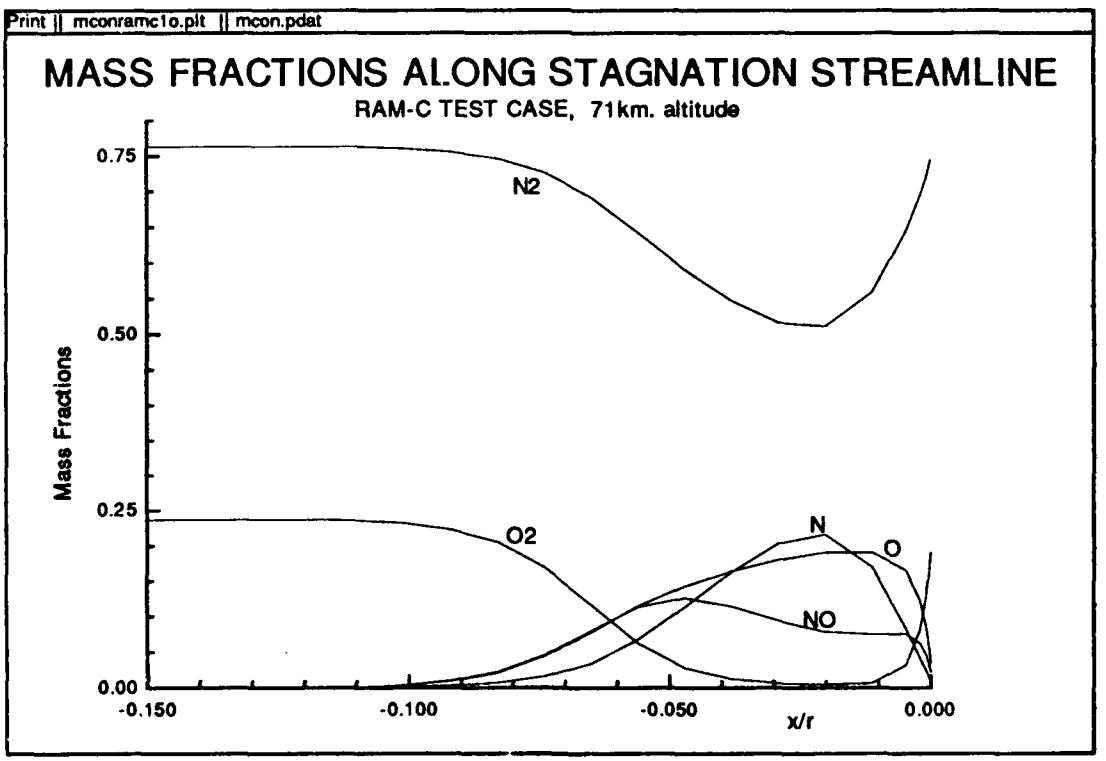

Fig.12 Stagnation streamline mass fractions, RAM-C II test case.

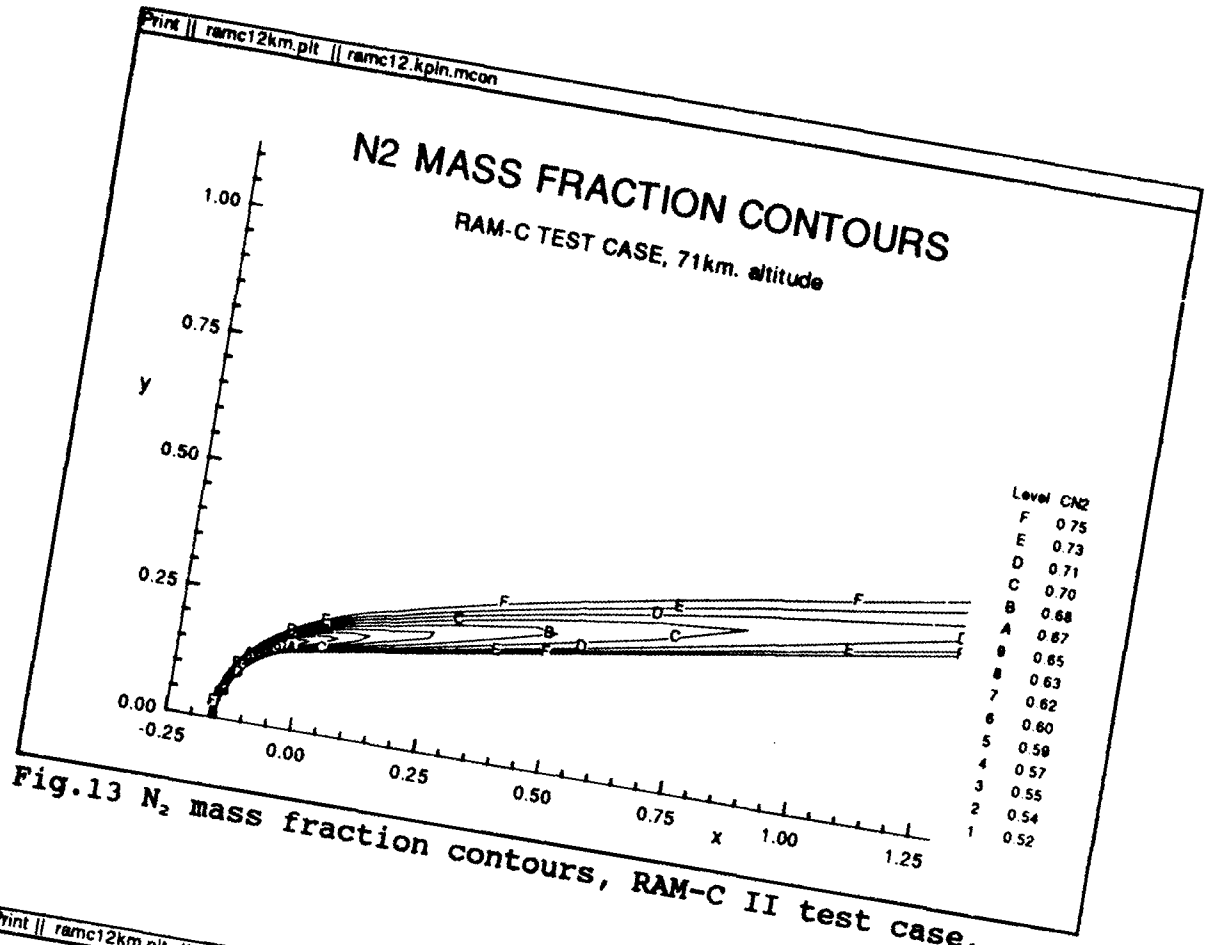

Fig.13 N_2 mass fraction contours, RAM-C II test case.

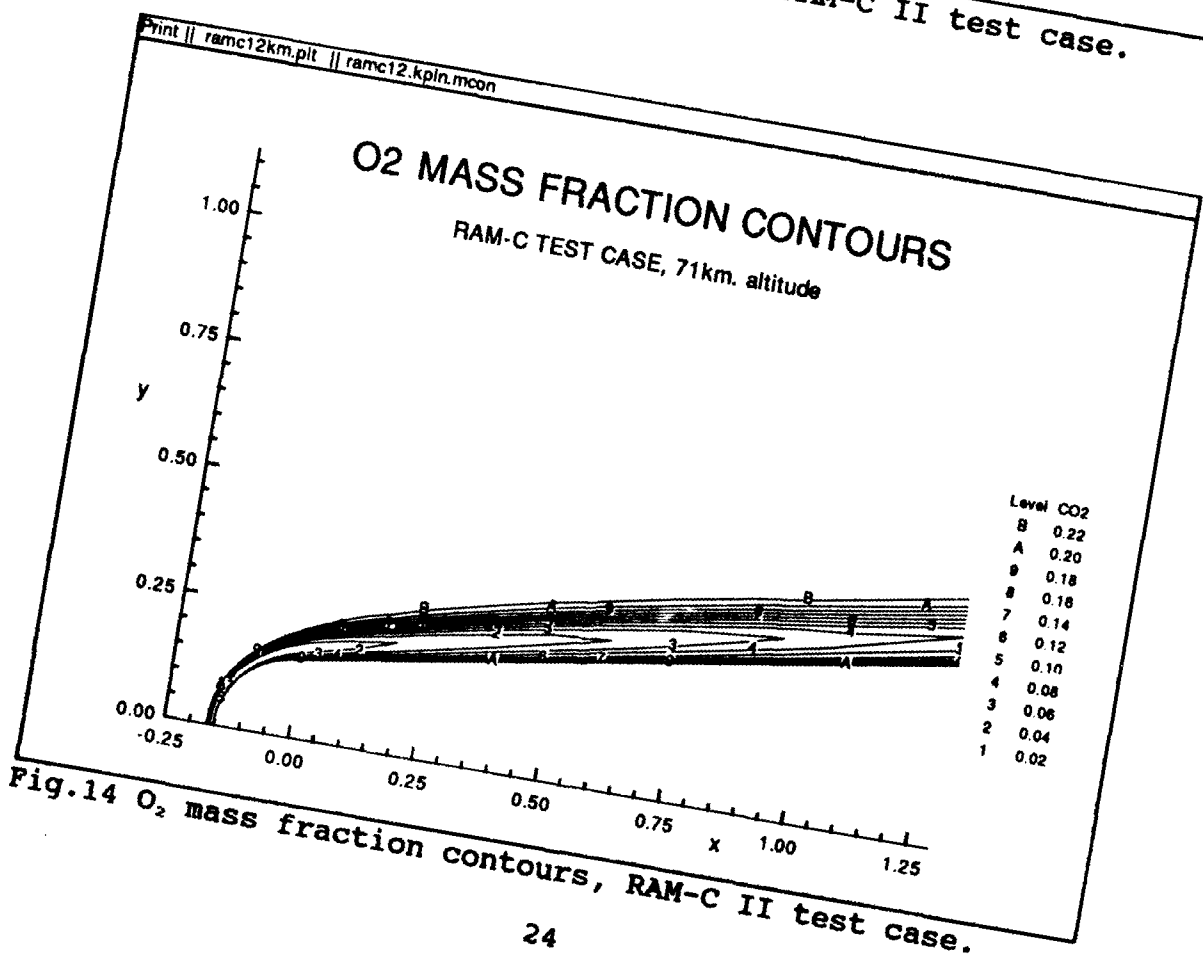

Fig.14 O_2 mass fraction contours, RAM-C II test case.

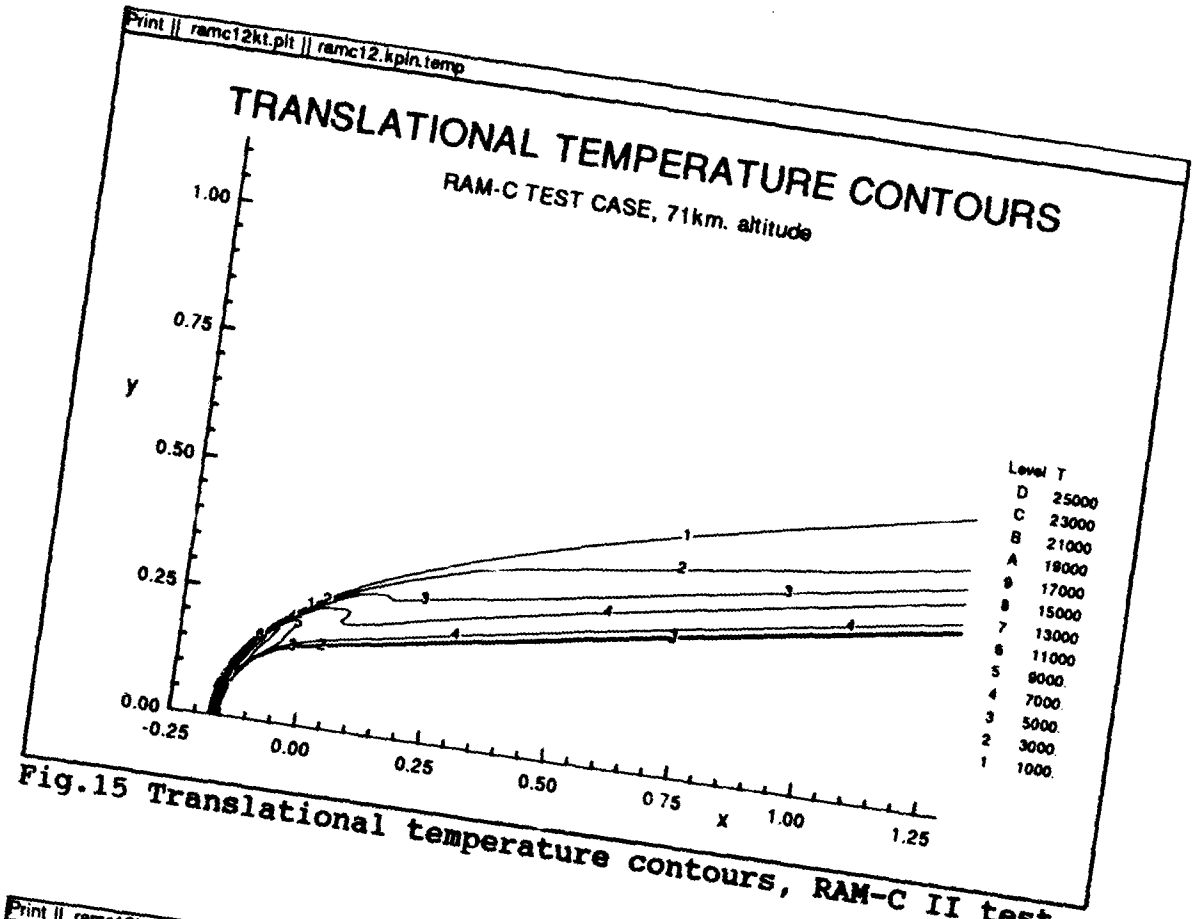

Fig.15 Translational temperature contours, RAM-C II test case.

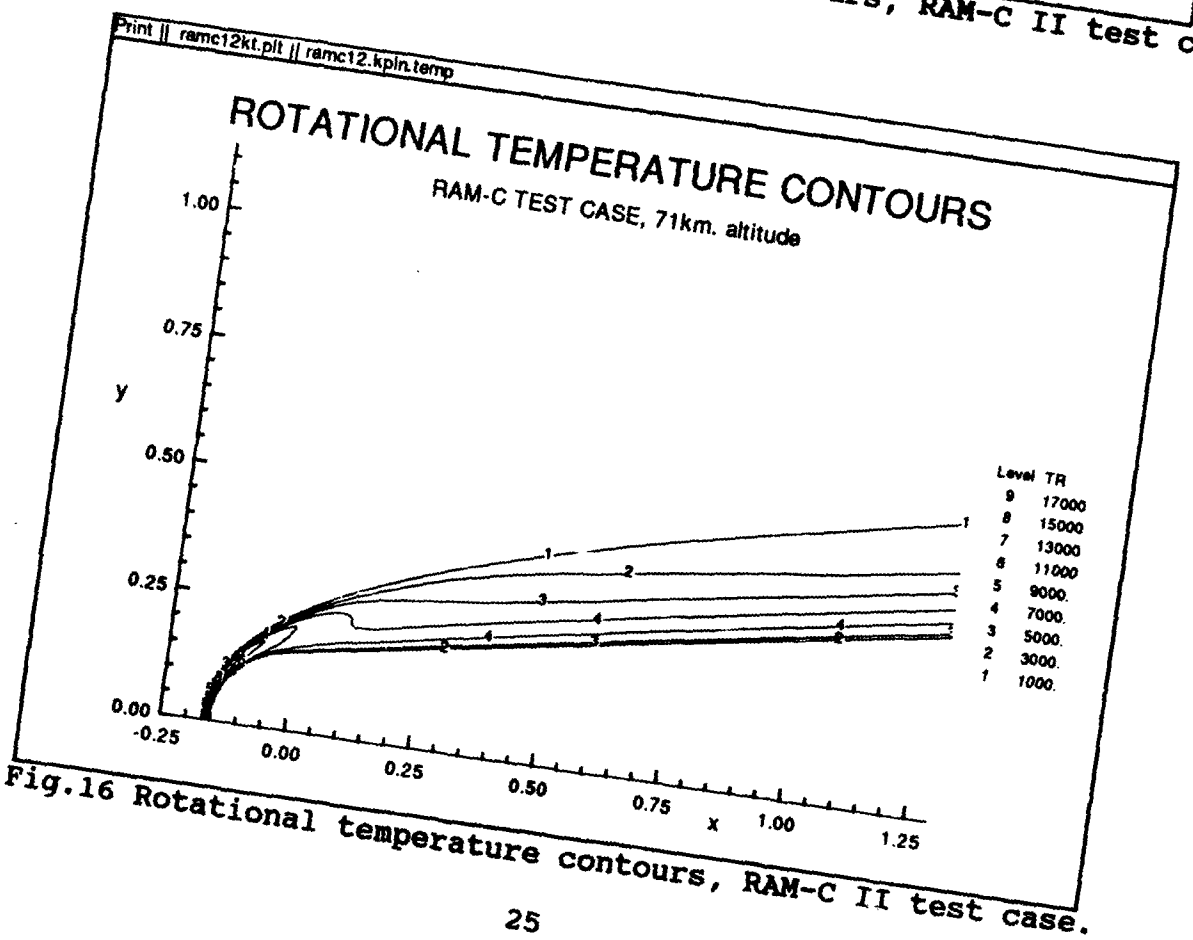

Fig.16 Rotational temperature contours, RAM-C II test case.

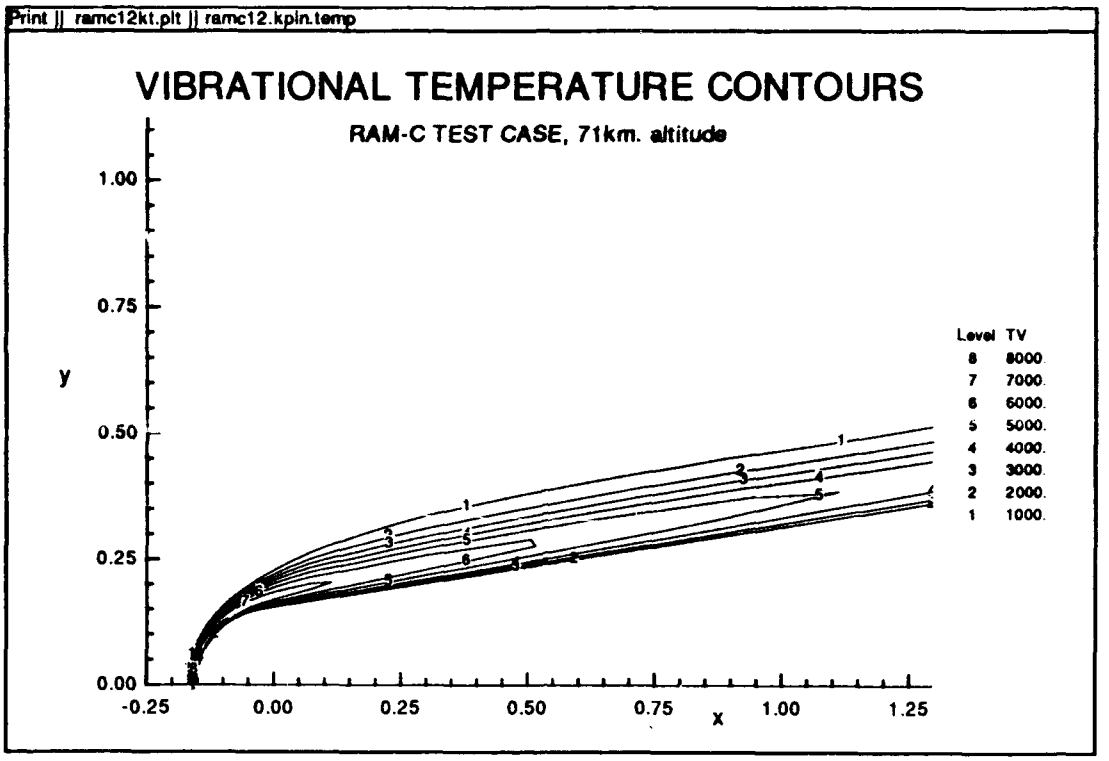

Fig.17 Vibrational temperature contours, RAM-C II test case.

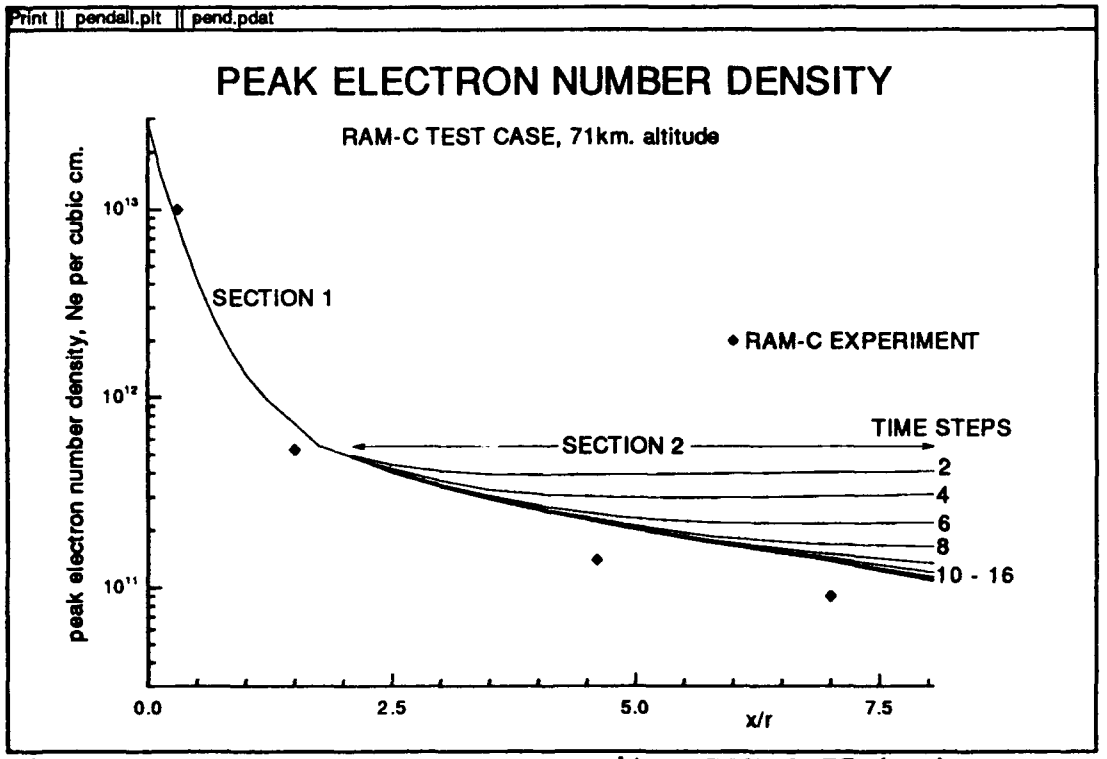

Fig.18 Peak electron number density, RAM-C II test case.

(3D) Print || ghvasrf.plt || srfdat.pdat

APPLICATION TO A GENERIC HYPERSONIC VEHICLE

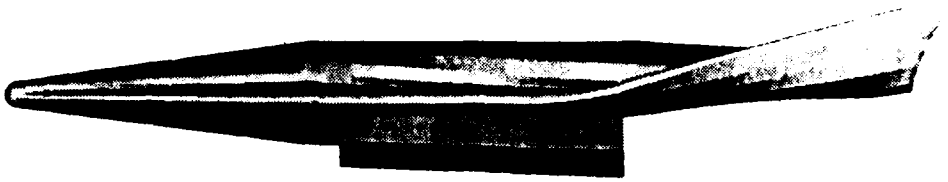

SPHERE-CONE-CYLINDER-DELTA WING-BODY

LENGTH = 71m., SPHERE RADIUS = 1m.

CYLINDER RADIUS = 4m.

CONE HALF ANGLE = 7.5 DEGREES

DELTA WING HALF ANGLE = 20 DEGREES

Fig.19 Generic hypersonic vehicle definition.

(3D) Print || ghvasrf.plt || srfdat.pdat

FLIGHT CONDITIONS

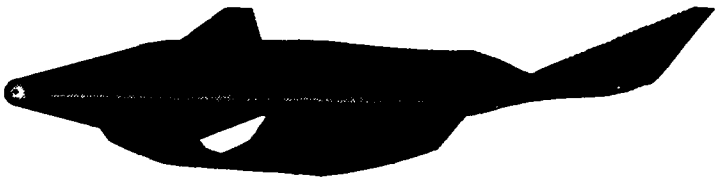

LEVEL FLIGHT AT 71km. ALTITUDE

MACH 25 LAMINAR FLOW

FREESTREAM PRESSURE 4.9 N/m**2

FREESTREAM TEMPERATURE 216 DEGREES K

BODY TEMPERATURE 1500 DEGREES K

Fig.20 Flight conditions for generic hypersonic vehicle.

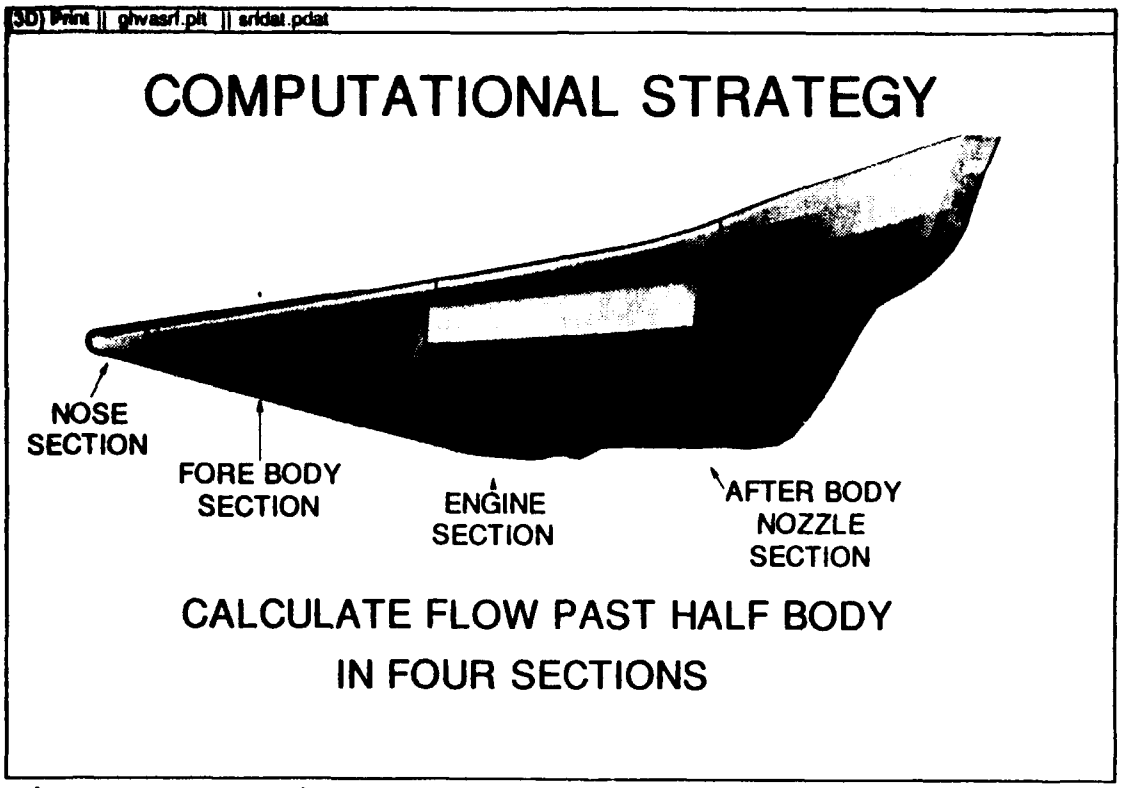

Fig.21 Computational strategy for hypersonic vehicle flow field.

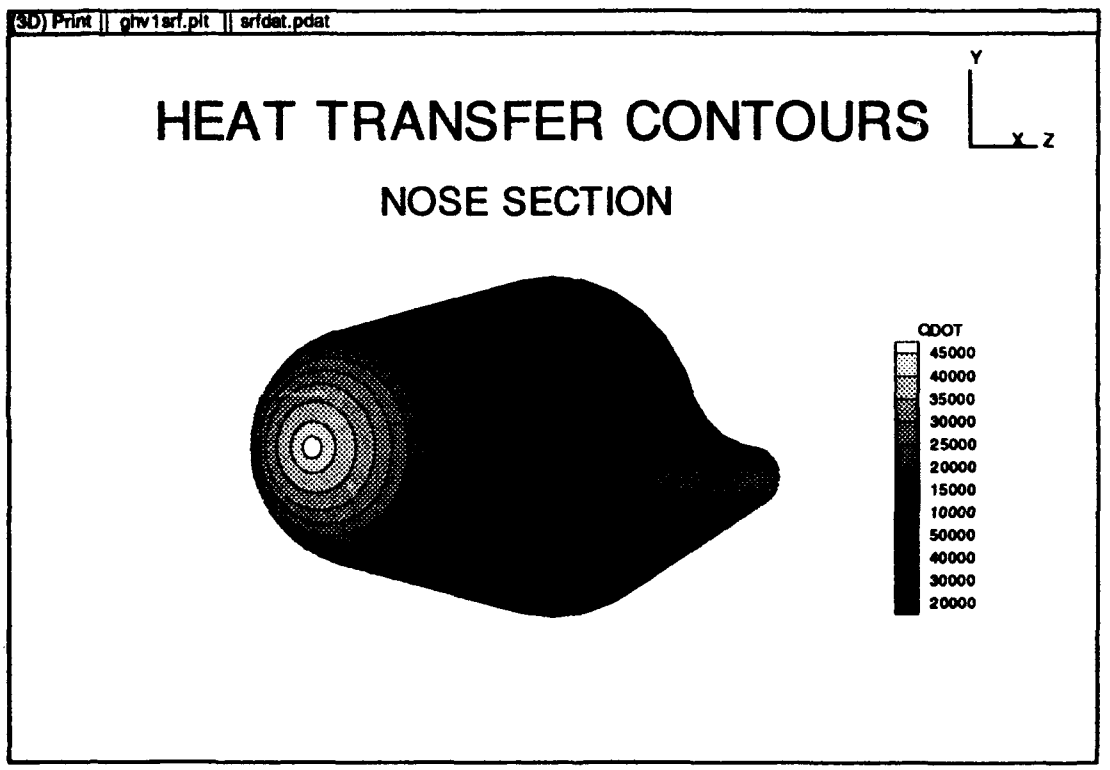

Fig.22 Heat transfer at nose section of hypersonic vehicle.

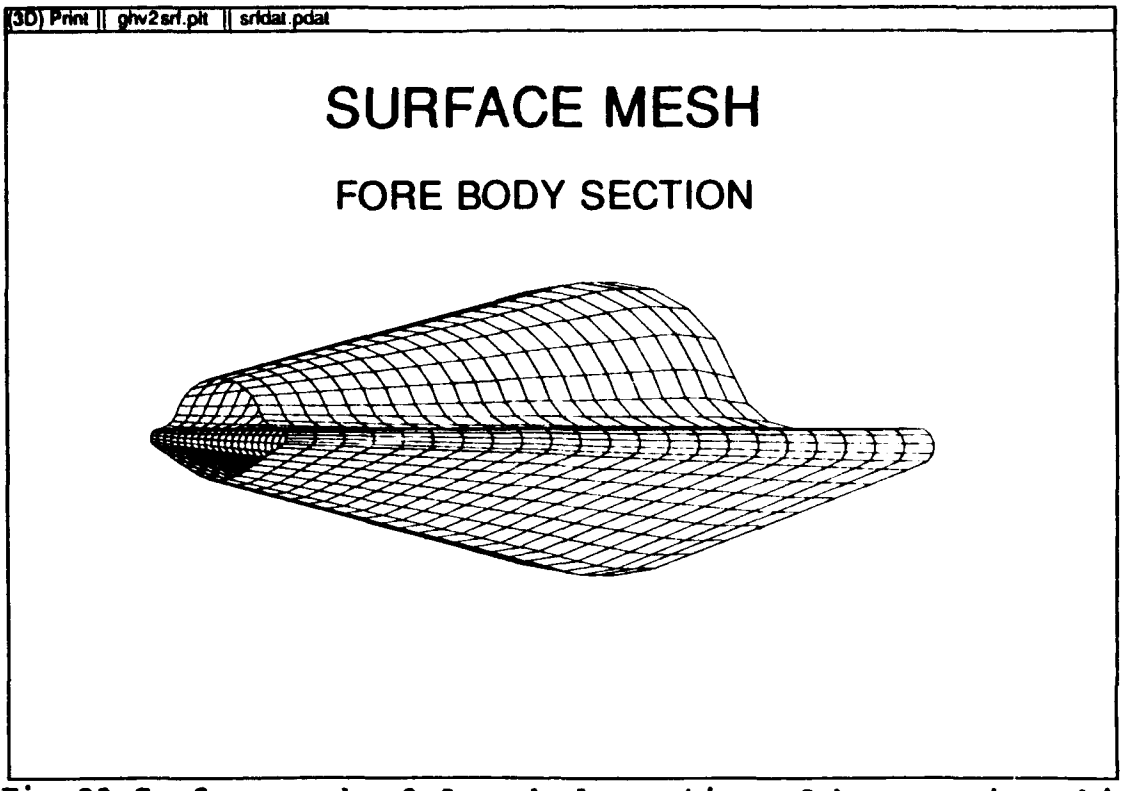

Fig.23 Surface mesh of fore body section of hypersonic vehicle.

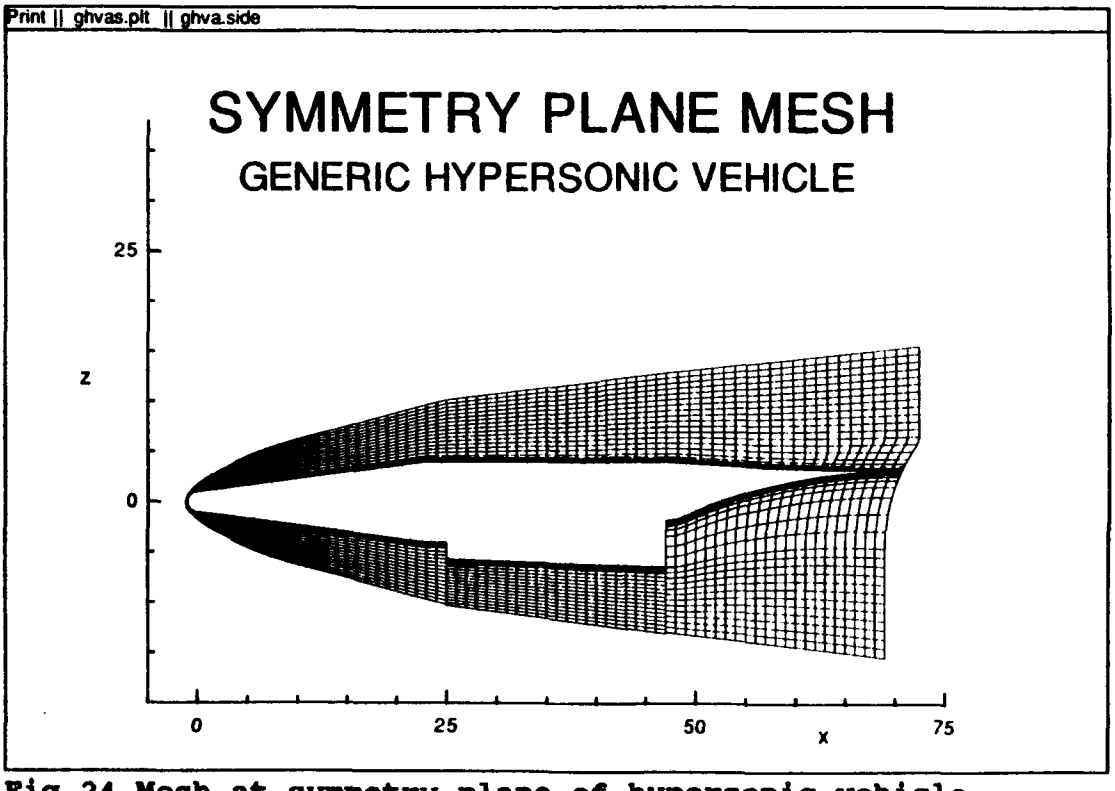

Fig.24 Mesh at symmetry plane of hypersonic vehicle.

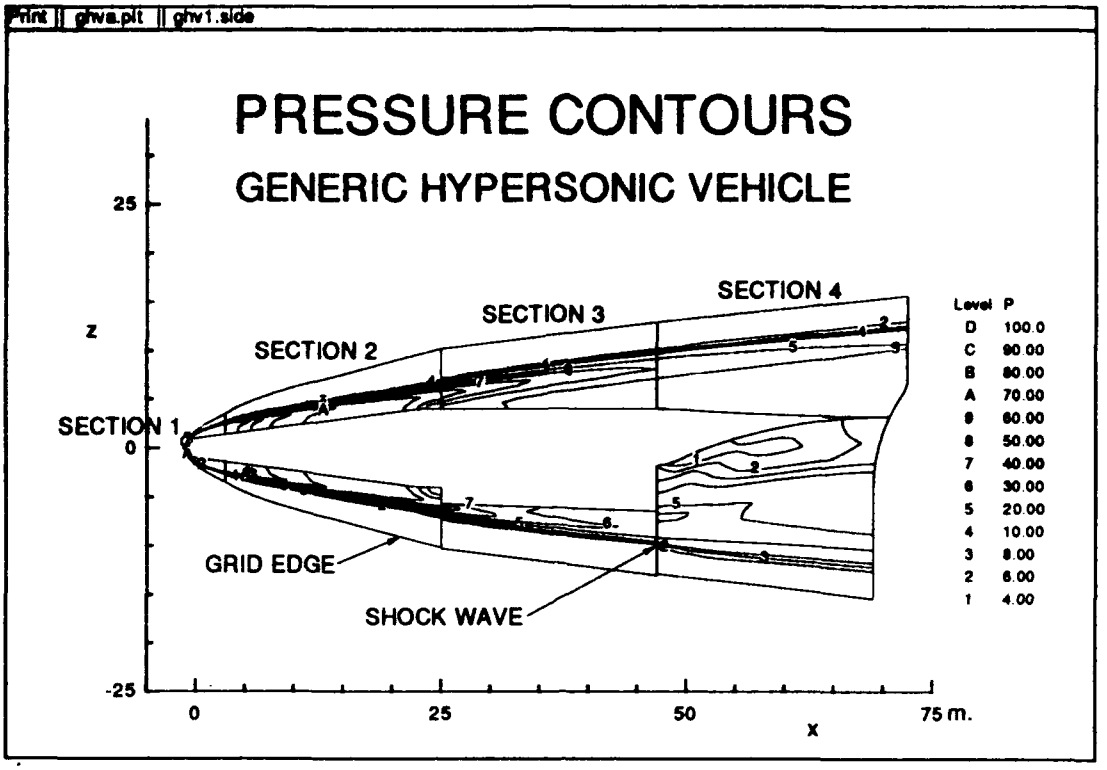

Fig.25 Pressure contours at symmetry plane of hypersonic vehicle.

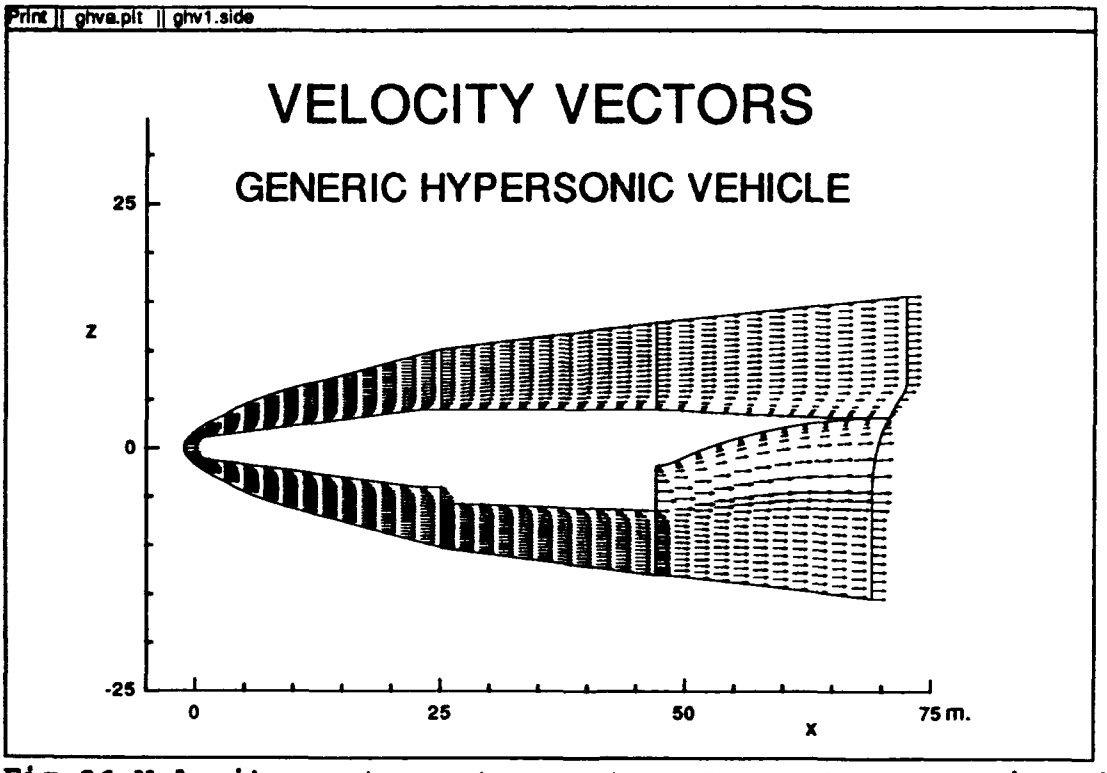

Fig.26 Velocity vectors at symmetry plane of hypersonic vehicle.

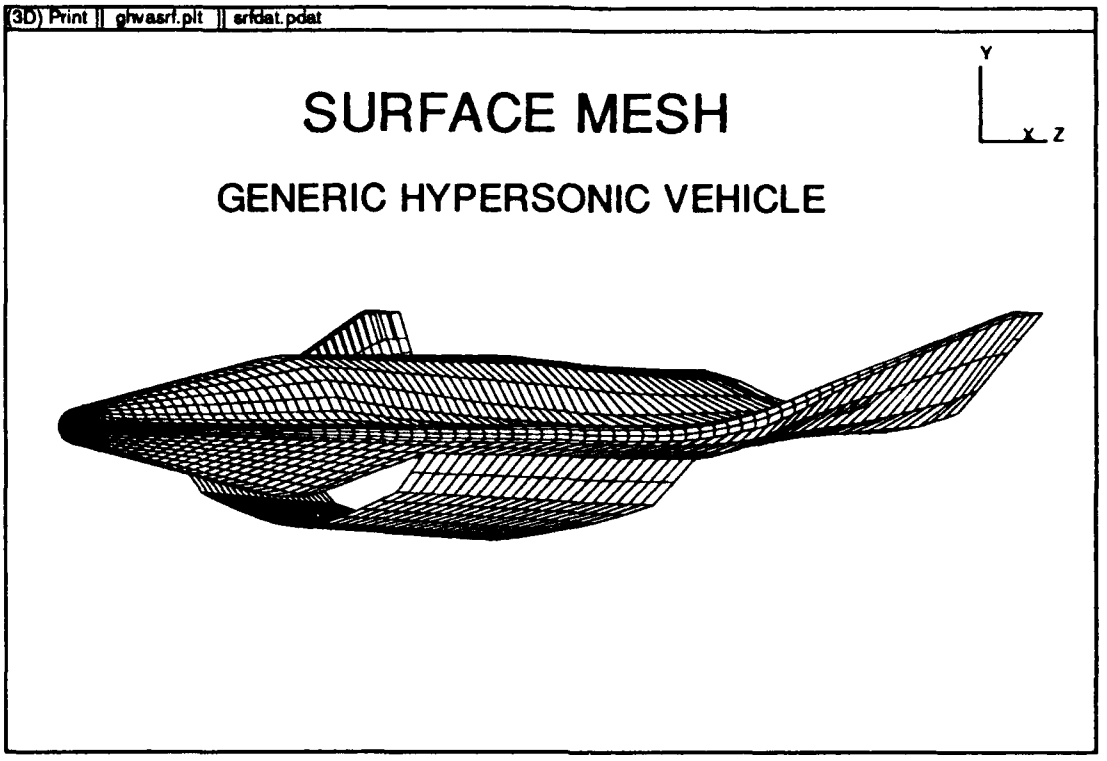

Fig.27 Surface mesh of hypersonic vehicle.

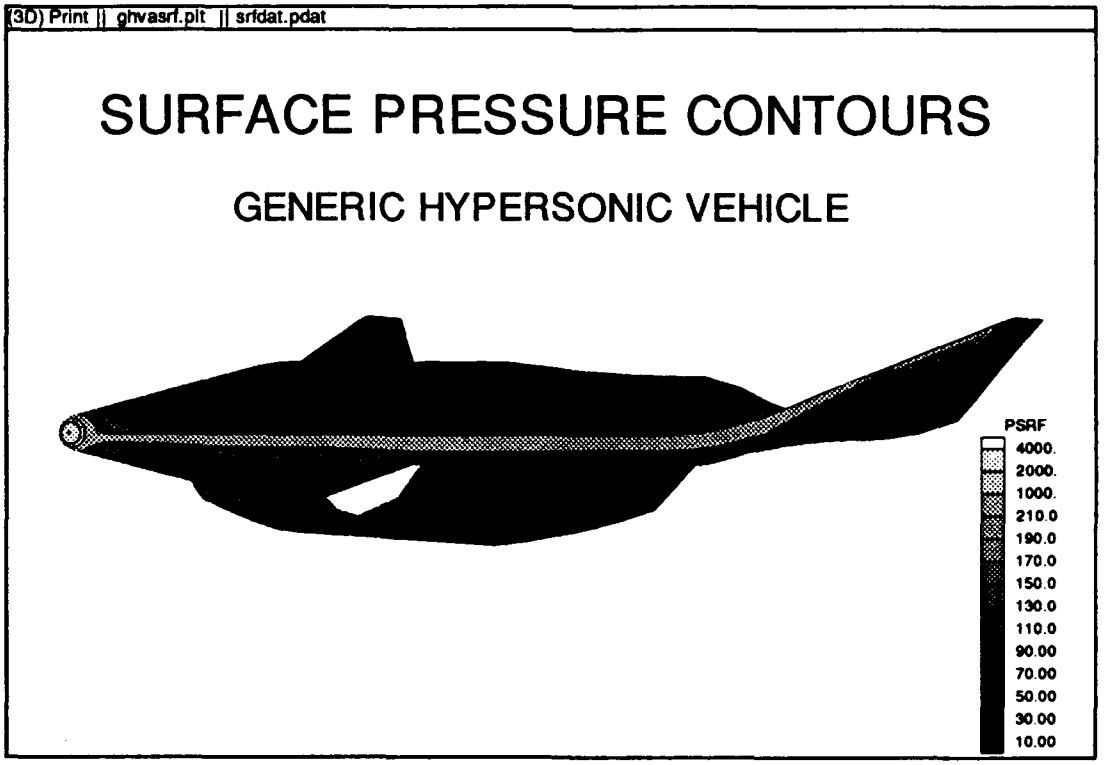

Fig.28 Surface pressure contours of hypersonic vehicle.

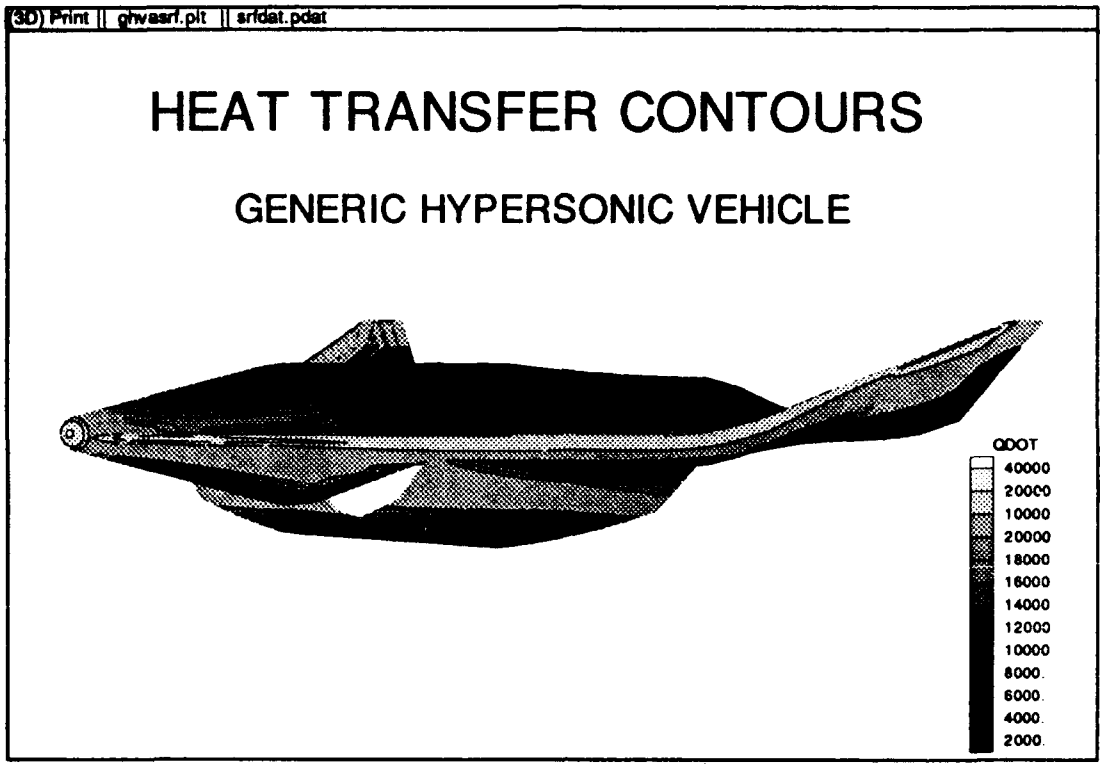

Fig.29 Heat transfer contours at surface of hypersonic vehicle.

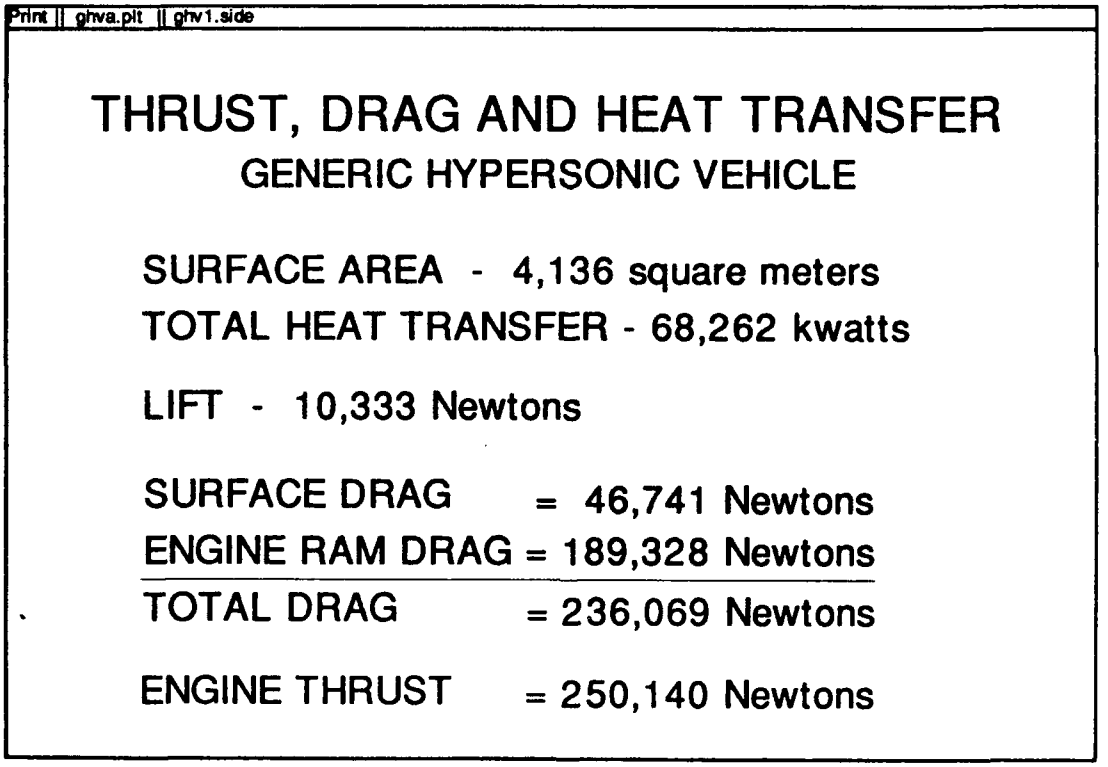

Fig.30 Thrust, lift, drag and heat transfer for hypersonic vehicle.

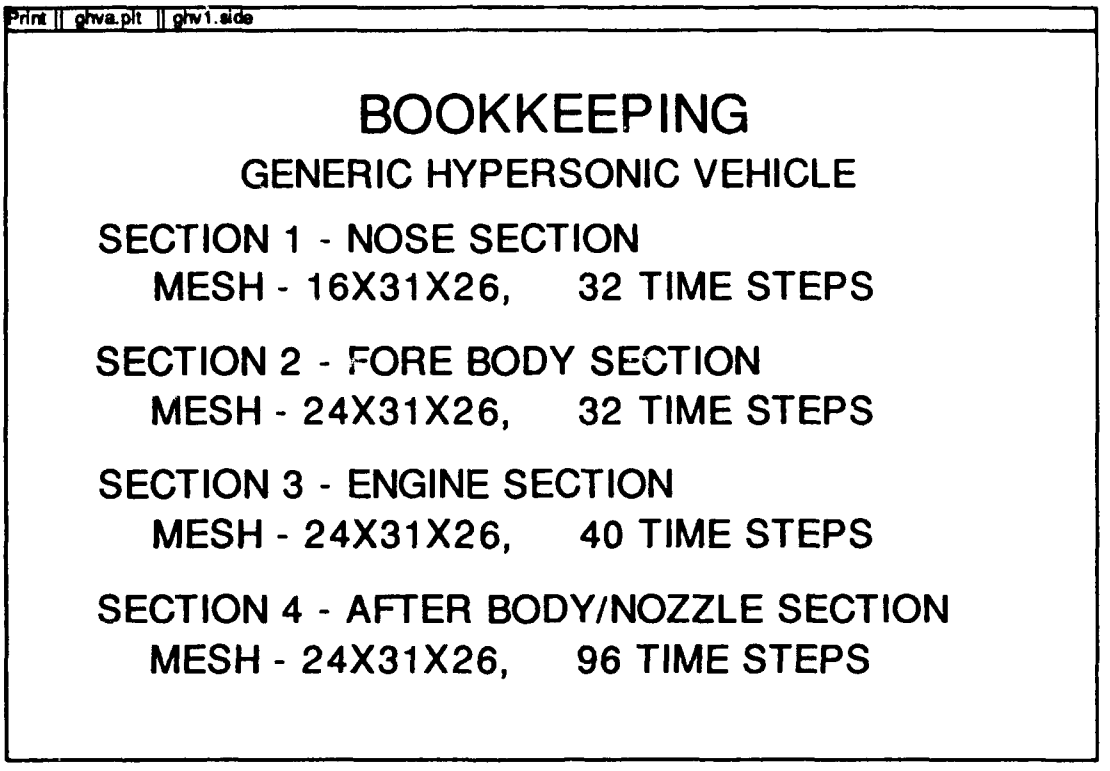

Fig.31(a) Section mesh sizes and time steps to convergence for numerical solution of flow past a generic hypersonic vehicle in powered flight.

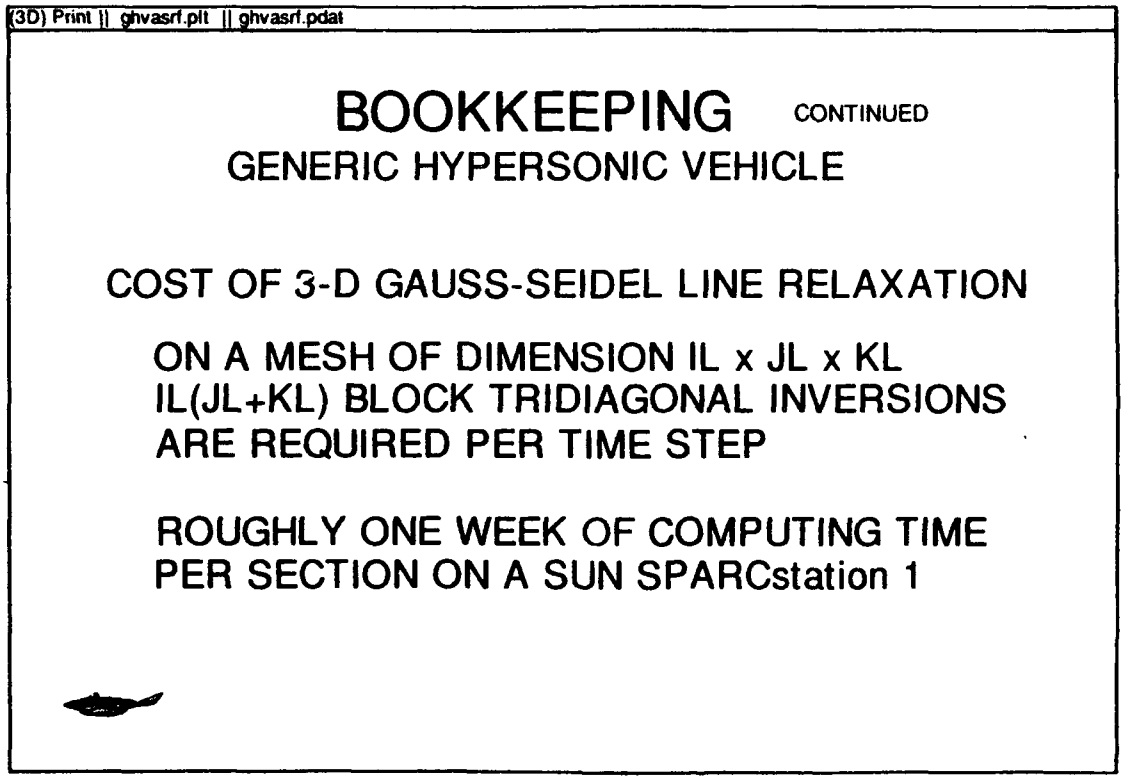

Fig.31(b) Computational cost of numerical solution for flow past a generic hypersonic vehicle in powered flight.

U.S. GOVERNMENT PRINTING OFFICE: 1993 - 550-106/80577